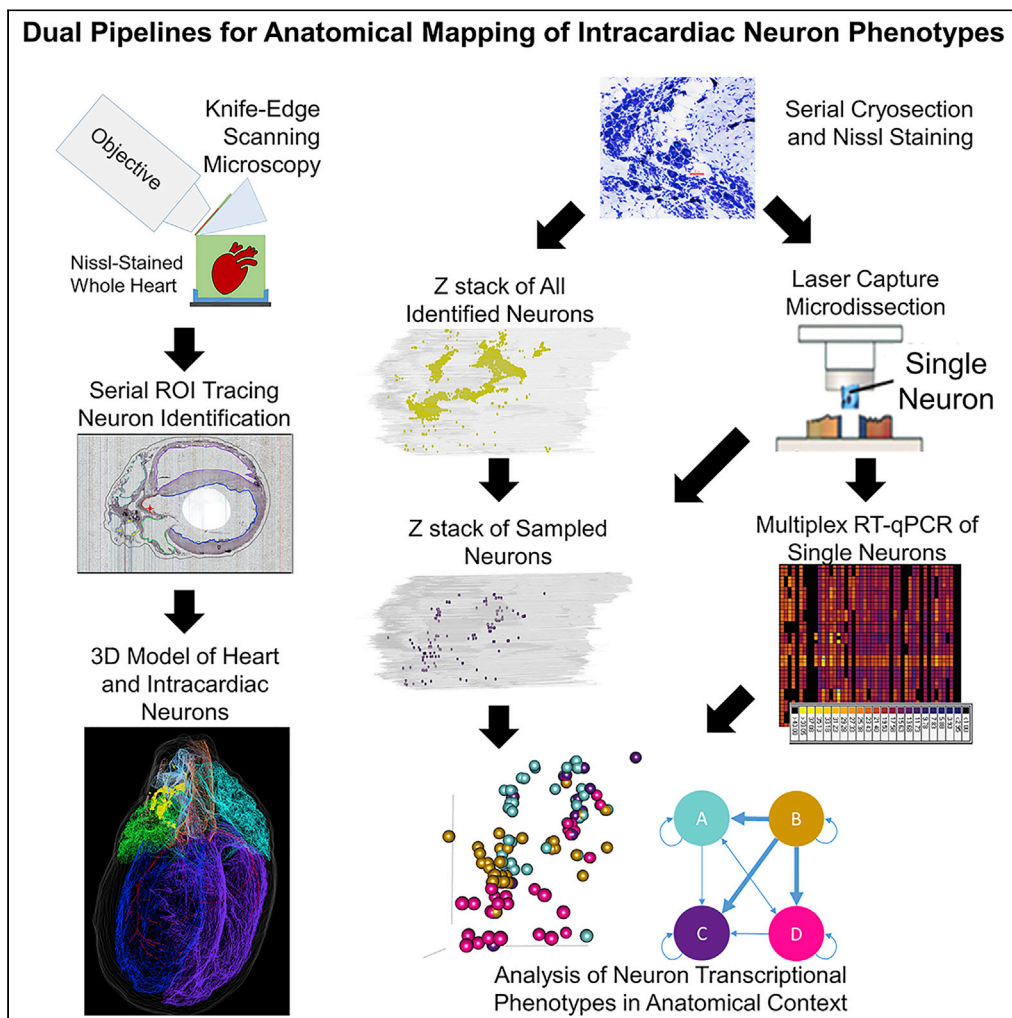


Article

A Comprehensive Integrated Anatomical and Molecular Atlas of Rat Intrinsic Cardiac Nervous System



Sirisha Achanta,
Jonathan Gorky,
Clara Leung, ...,
Zixi (Jack) Cheng,
Rajanikanth
Vadigepalli,
James S.
Schwaber

zixi.cheng@ucf.edu (Z.C.)
rajanikanth.vadigepalli@
jefferson.edu (R.V.)
james.schwaber@jefferson.
edu (J.S.S.)

HIGHLIGHTS

Comprehensive single-
neuron-scale mapping of
the intrinsic cardiac
nervous system

Whole-organ high-
throughput imaging and
reconstruction at a cellular
resolution

3D anatomical framework
for spatially tracked
single-neuron molecular
phenotypes

Integrated histology,
neuron mapping, and
molecular profiles for 3D
organ reconstruction

Achanta et al., iScience 23,
101140
June 26, 2020 © 2020 The
Authors.
[https://doi.org/10.1016/
j.isci.2020.101140](https://doi.org/10.1016/j.isci.2020.101140)

Article

A Comprehensive Integrated Anatomical and Molecular Atlas of Rat Intrinsic Cardiac Nervous System

Sirisha Achanta,^{1,5} Jonathan Gorky,^{1,5} Clara Leung,^{2,5} Alison Moss,^{1,5} Shaina Robbins,^{1,5} Leonard Eisenman,¹ Jin Chen,² Susan Tappan,³ Maci Heal,³ Navid Farahani,⁴ Todd Huffman,⁴ Steve England,⁴ Zixi (Jack) Cheng,^{2,*} Rajanikanth Vadigepalli,^{1,*} and James S. Schwaber^{1,6,*}

SUMMARY

We have developed and integrated several technologies including whole-organ imaging and software development to support an initial precise 3D neuroanatomical mapping and molecular phenotyping of the intracardiac nervous system (ICN). While qualitative and gross anatomical descriptions of the anatomy of the ICN have each been pursued, we here bring forth a comprehensive atlas of the entire rat ICN at single-cell resolution. Our work precisely integrates anatomical and molecular data in the 3D digitally reconstructed whole heart with resolution at the micron scale. We now display the full extent and the position of neuronal clusters on the base and posterior left atrium of the rat heart, and the distribution of molecular phenotypes that are defined along the base-to-apex axis, which had not been previously described. The development of these approaches needed for this work has produced method pipelines that provide the means for mapping other organs.

INTRODUCTION

In recent years neuroanatomy research in mammalian brain has come to the forefront (e.g., in the NIH Brain Initiative, Blue Brain Project, and Connectome Project), dependent on the development of three-dimensional (3D) digital reference atlases at the cellular scale. This has revealed the complex diversity of the molecular phenotypes of neurons, often showing orderly spatial gradients of neuron types (e.g., work from the David Van Essen laboratory and the Allen Institute). In this report we further develop and extend these approaches to bring them to bear on the rodent intrinsic cardiac nervous system (ICN). Here, we present a comprehensive 3D mapping of rat ICN distribution in the overall histological and ontological context of the heart while demonstrating anatomically specific single-neuron transcriptional gradients. We herein show the development, coordination, and integration of several technologies including whole-organ imaging, software development, precise 3D neuroanatomical mapping, and molecular phenotyping. The development of the approaches needed to acquire these data has produced two method pipelines that can achieve the goals of the National Institutes of Health Common Fund's Stimulating Peripheral Activity to Relieve Conditions (SPARC) program: Comprehensive Functional Mapping of Neuroanatomy of the Heart.

Autonomic control of cardiac function arises from several integrative centers in the central nervous system, but the final level of neural integration controlling cardiac function lies in the ICN. Although the heart is known to possess a significant population of neurons, these have not previously been mapped precisely as to their number or extent/position/distribution while maintaining the histological context of the whole heart. This 3D neuroanatomical information is necessary to understand the connectivity of the neurons of the ICN and to develop their functional circuit organization. Mapping of molecular phenotypes and cell functions must also occur in the anatomical context to ensure a holistic comprehension of ICN.

Prior mapping efforts of ICN in small animals have included: mouse (Li et al., 2010, 2014; Rysevaite et al., 2011a), rat (Ai et al., 2007; Cheng et al., 1999, 2004; Cheng and Powley, 2000), rabbit (Saburkina et al., 2014), guinea pig (Hardwick et al., 2014; Steele et al., 1994), and human (Armour et al., 1997). Some of these

¹Daniel Baugh Institute for Functional Genomics/Computational Biology, Department of Pathology, Anatomy, and Cell Biology, Thomas Jefferson University, Philadelphia, PA, USA

²Burnett School of Biomedical Sciences, College of Medicine, University of Central Florida, Orlando, FL, USA

³MBF Bioscience, Williston, VT, USA

⁴Strateos, San Francisco, CA, USA

⁵These authors contributed equally

⁶Lead Contact

*Correspondence: zixi.cheng@ucf.edu (Z.C.), rajanikanth.vadigepalli@jefferson.edu (R.V.), james.schwaber@jefferson.edu (J.S.S.)

<https://doi.org/10.1016/j.isci.2020.101140>



prior efforts provided limited mapping. Others represented gross staining of neurons with coarse-grain graphical representations of the areas involved. Although qualitative and gross anatomical descriptions of the ICN have been presented earlier, we present here a comprehensive neurocardiac atlas of the ICN in rat at cellular and molecular levels at a microscopic level.

The present datasets are a revelation of previously unsuspected complexity and diversity of modulators, receptors, and neurotransmitters that is already stimulating new anatomical and functional studies. The present discovery of phenotypical spatial gradients will stimulate connectomic studies to associate these with cardiac targets and functions going forward. Such work will ultimately be important for cardiac electrophysiologists performing ablation procedures. Prior work could not and did not relate cell-scale neuroanatomy and cardiac-scale organ anatomy, which our present results do. There is no prior literature on ICN transcriptomics or localization. This will be invaluable to researchers and clinicians including, but not limited to, autonomic nervous system investigators, vagus nerve cardiac regulation investigators, vagus nerve therapy investigators, cardiologists, and heart anatomists.

RESULTS

Multidisciplinary Approach to Data Acquisition Pipelines

We developed and applied a dual method pipeline to create a comprehensive anatomical map and molecular profile, within the 3D structure, of cardiac neurons in a rat heart. We combined a diverse set of technologies that enabled a geographically distributed network of researchers with distinct skills to coordinate and enable the present results. These data acquisition approaches are graphically represented in the two pipelines in [Figure 1](#). In the pipeline represented in [Figure 1A](#) we used knife-edge scanning microscopy (KESM) to image and retain the 3D structure of the heart. In parallel, custom software was used to assemble and compress the resulting ~750,000 individual images to generate a single image volume. Annotation of the resulting image for mapping the ICN in the histological context of the whole heart was performed with Tissue Mapper, a software created for this purpose.

A second pipeline demonstrates the acquisition of neurons as single-cell-scale samples after cryostat sectioning of the heart to ascertain circuit connectivity and molecular phenotypes using transcriptional profiling ([Figure 1B](#)). Then the molecular phenotype(s) of these neurons can be placed in whole heart and ICN anatomical context. Images of these sections, including neuronal positions, are registered and aligned using Tissue Maker to create a whole heart volume with neuronal phenotype data that can be brought into the 3D reference system created by the first approach thus generating single-cell transcriptomics in a robust anatomical context that can incorporate data from multiple subjects for future comparison.

Comprehensive Neuroanatomy of the Rat Heart

Heart tissue sections were imaged as they were cut using a fourth-generation KESM platform, preserving tissue section morphology and registration to precisely conform to that of the intact, paraffin-embedded organ. The image resolution (0.5 μm per pixel) yields clear visualization of cellular/neuronal-scale histology. The registration and stacking of all the section images is in a format compatible with the purpose-built software, TissueMaker and Tissue Mapper, which supports using the latter to precisely map the position of each neuron and histological features of the heart and blood vessels from each tissue section. We then combine the positions of all neurons and features of cardiac tissues using computer graphics to hold all the data as a precise 3D representation of that specific heart's ICN distribution in the histological context of the heart. The representation is precise and reproducible because both the tissue image acquisition and the mapping of neurons and cardiac features are under sub-micron control. This data acquisition pipeline is presented in [Figure 1A](#). The complete dataset of anatomical mapping is available online via SPARC Data Portal (<http://data.sparc.science>).

As we take such care to represent the exact positions of all the neurons in a precisely preserved heart-organ morphology, we now can interact with the 3D model presenting all the mappings in various formats, scales, or representations to appreciate the neuroanatomy of the ICN, enabling the following analyses:

- As illustrated in [Figure 2](#) the ICN distribution is seen in the context of the whole 3D heart, depicting the unexpectedly extensive distribution of neurons on both posterior atria extending in the superior-inferior dimension from the base of the heart to the coronary sulcus or atrioventricular groove.

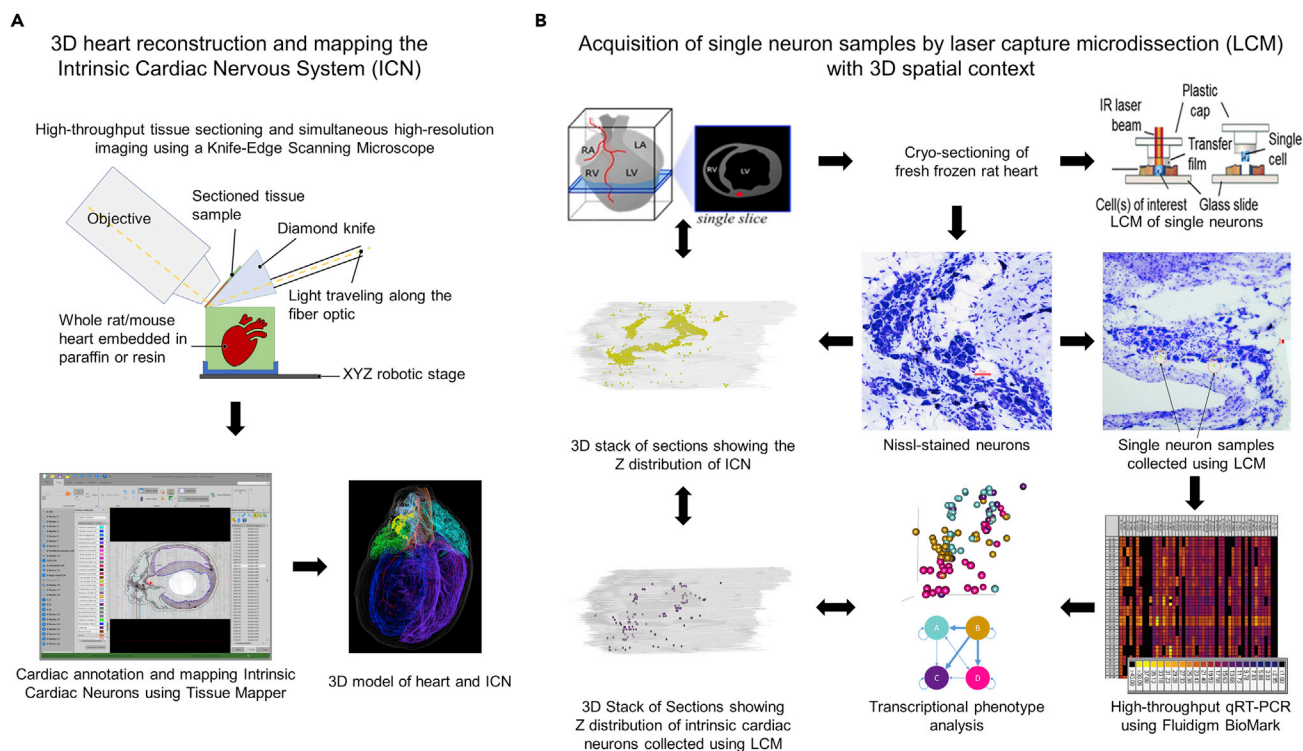


Figure 1. Data Acquisition Pipelines

(A) Acquisition of a 3D, accurate organ reference framework using high-resolution collection of histological tissue sections. Once the entire heart is sectioned and imaged, the images are then compiled into an image volume by the TissueMapper software to enable 3D heart reconstruction and ICN mapping with the TissueMapper software.

(B) Acquisition of cresyl violet-stained neuronal samples from fresh heart tissue by cryostat sectioning. Single neurons were identified by position in the ICN and lifted for qPCR or RNA-seq molecular phenotyping.

- We are also able to view subsets of the ICN in their local heart context by restricting the 3D model using the “partial projection” software tool. For example, [Figure 3](#) is a 3-mm sagittal section representing neurons along the superior-inferior extent of the heart. [Figure 4B](#) creates a 3-mm-thick section in the transverse plane that visualizes neurons located on the base/hilum of the heart. In contrast, [Figure 5](#) excludes these neurons showing only the more inferiorly positioned neurons.
- We are able to describe the exact position of ICN neurons in histological sections. [Figure 6](#) consists of single sagittal section views of neurons throughout the superior-inferior extent in a series of sections going from the right to the left side of the heart.
- The digital neuron mapping supports quantitative analyses of neuron distributions and packing density as illustrated in [Figure 7](#).
- These above-mentioned anatomical templates support addition of connectome and molecular identity data. [Figure 8](#) shows the neurons in the digitized high-resolution images of histological sections. [Figures 8](#) and [9](#) illustrate the strategy used in which we employed the pipeline represented in [Figure 1B](#), to laser capture single neurons for molecular analysis. [Figure 10](#) visualizes the mapped ICN distribution to the distribution of neurons sampled and analyzed for molecular phenotypes. [Figures 11, 12, and 13](#) present analyses of molecular neuronal phenotypes, and demonstrate the gradients and distribution of phenotypes across the extent of the ICN.

The results from these visual and quantitative analyses are presented in detail in the following section. In addition to the figures, the visualizations are also represented in movies available in the [Supplemental Information](#).

We sought to delineate the distribution, extent, and location of neurons on the heart in part by the use of 3D graphical models of the ICN in cardiac context both in figures and by rotating the model ([Video S1](#)).

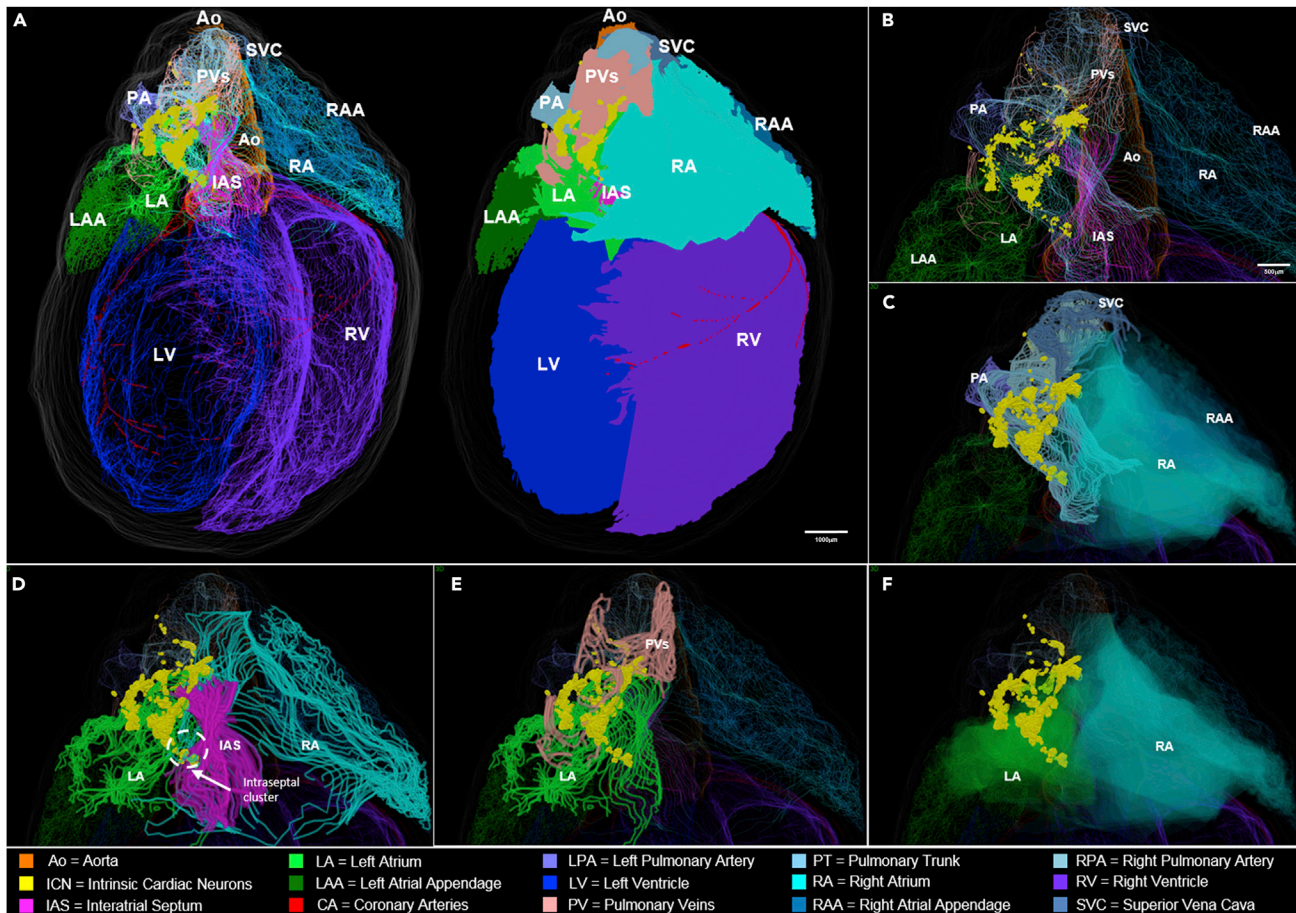


Figure 2. Posterior View of the 3D Reconstructed Male Rat Heart

(A) Whole-heart view showing the context, extent, and distribution of the intrinsic cardiac neurons (ICN), located on superior and posterior surfaces of the atria.

(B–F) A higher-resolution view of the atria and blood vessels that are shown in (B), with various contoured features of heart anatomy that are selectively removed to appreciate the anatomical relationship of the ICN to (C) the pulmonary artery and superior vena cava (SVC), (D) the interatrial septum, (E) the left atrium and pulmonary veins, (F) the right atrium, where clusters #1 and #2 appear to be on the surface of both atria, whereas cluster #3, which is located around the border of the superior vena cava, left atrium, and right atrium, appears on the right atrium. (See also [Video S2](#)). Scale bars: panel A, 1000 μm ; panels B–F, 500 μm .

Examining the 3D model framework of the ICN from a posterior point of view shows the entire population as compact and localized to a region on the superior and posterior aspects of both left and right atria, extending inferiorly to the atrioventricular boundary or the coronary sulcus at the boundary with the ventricles, as seen in [Figure 2A](#) (also see [Video S2](#)). The additional panels, [Figures 2B–2F](#), are enlarged images of select regions of the heart to highlight the anatomical features of ICN, in each of which various contours outlining specific features of cardiac anatomy are dimmed. This provides a better appreciation of the ICN distribution, shape, extent, and location in relation to specific cardiac structures. With all contours illuminated the zoomed-in ICN appears to comprise three or more large clusters in which neurons extend rostral to caudal almost continuously ([Figure 2B](#)). At its most superior extent, portions of the ICN lie adjacent, semi-surrounding, and posterior to the pulmonary artery and superior vena cava, on the right side of the heart ([Figure 2C](#)). As neurons extend inferior to these levels they distribute in the shape of “a comma” and extend laterally to the left. Neurons at these levels are situated on both atria and within the interatrial septum (IAS) ([Figure 2D](#)). Further inferior the ICN neurons can be seen to distribute in relation to the contours of the pulmonary veins in [Figure 2E](#), extending on the posterior surface of the left atrium to the boundary with the left ventricle. In summary, the 3D reconstruction illustrates how the most prominent clusters of neurons are positioned on the left atrium and/or across both atria as in [Figure 2F](#). Most neurons appear to be located on the posterior surface of the left atrium. Other neurons, more superiorly located,

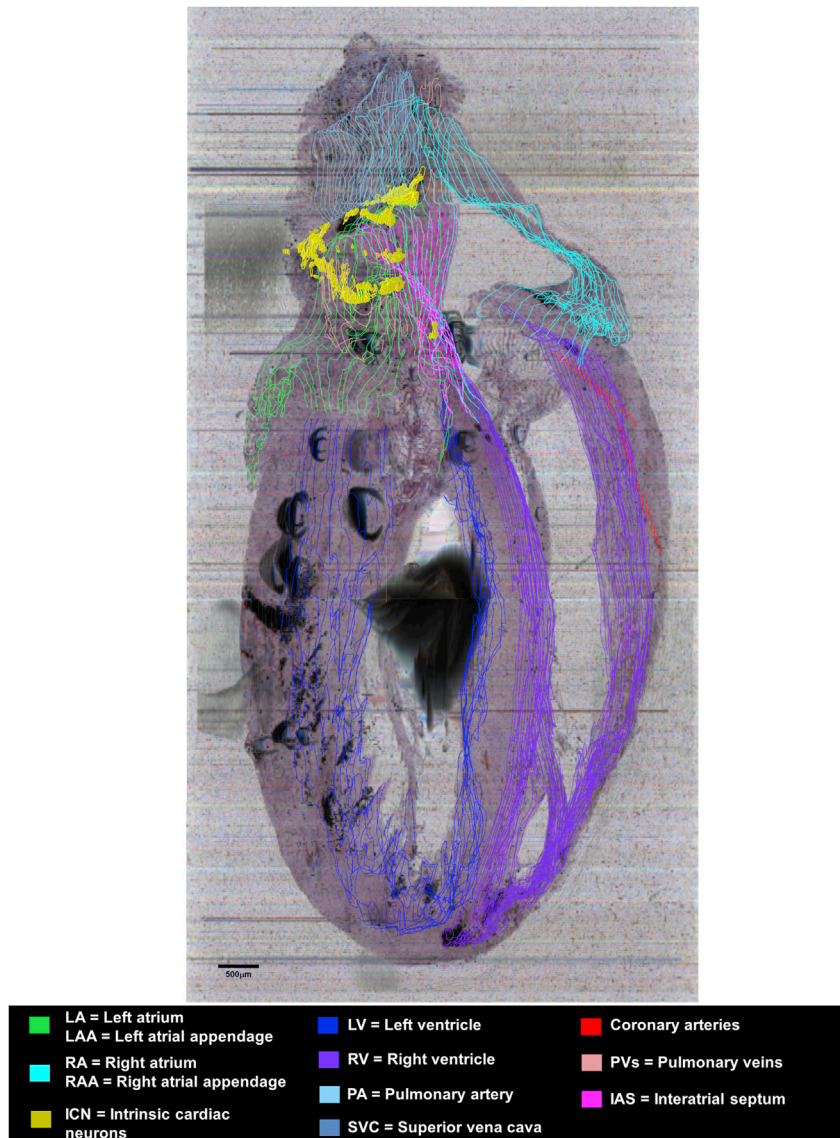


Figure 3. ICN Distribution in a Partial Projection of Sagittal Heart Sections

A partial projection of contours and ICN in a 3-mm-thick sagittal image slab illustrates the distribution of neurons along the superior-inferior extent of the heart. Scale bar: 500 μ m.

are located within the IAS and on the right atrium. This again shows that the ICN is associated with the posterior wall of both left and right atria as well as the IAS (Ai et al., 2007; Cheng et al., 1999, 2017). Using visual inspection for grouping, there are three large clusters of ICN neurons associated with the atria denoted as #1, #2, and #3. From this perspective, clusters #1 and #2 appear to be principally on the epicardial surface of the left atrium, whereas cluster #3, located adjacent to the borders of the superior vena cava, left atrium, and right atrium, appears to be largely on the right atrium.

The ICN distributes on the posterior atria. To position, in higher resolution, the neurons associated with posterior cardiac structures, we used the virtual section “partial projection” tool from the Tissue Mapper software. Using partial projection, a user-defined subset of the 3D heart model and neurons in any plane and thickness can be displayed, more than single sections and less than the full 3D model. Using this tool we made a virtual section that displays only neurons in a 3-mm sagittal section oriented superior-inferior, centered on the posterior cardiac surface, as seen in Figure 3. This shows a more restricted portion of the heart structure while presenting a more coherent view than single sections can provide. At these levels the

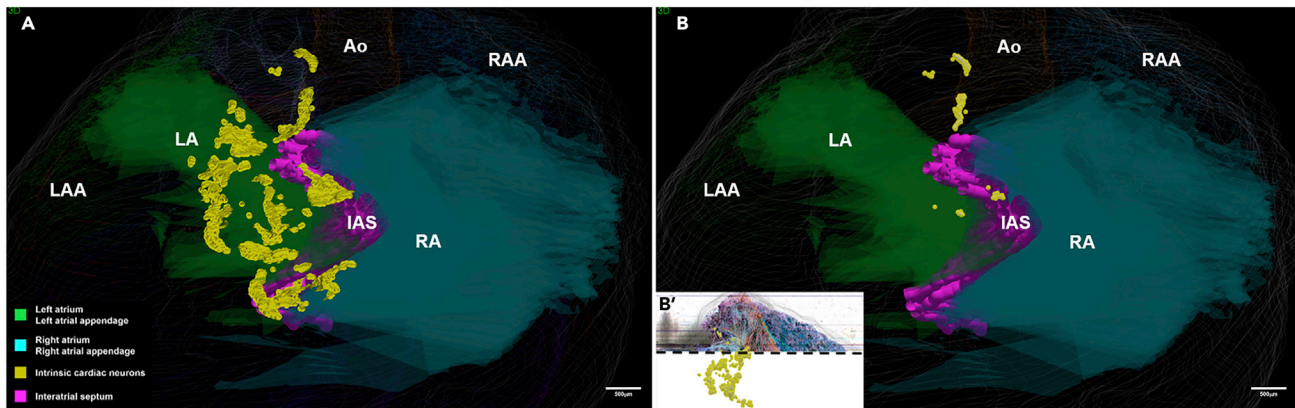


Figure 4. Superior View of the ICN

(A and B') (A) Viewing the ICN distribution (neurons mapped as yellow dots) looking from the base toward the apex. The left and right distribution of all ICN neurons is discriminated by their relationship to the interatrial septum. Note that most ICN neurons visualized in (A) are not all on the base of the heart but mostly distributed at more inferior-caudal levels of the heart on both atria. (B') To selectively view those neurons on the base of the heart we took this posterior view of the full ICN and retained only those above the cutoff point indicated by the dotted black line. (B) Then these neurons are here observed from the superior view of the heart, showing the position of ICN neurons located within the hilum in between the aorta, superior vena cava, and pulmonary artery. (See also [Video S3](#)). Scale bars: 500 μ m.

majority of neurons appear inferior to the base of the heart, extending to the coronary sulcus. This thick section and point of view is focused on the posterior surface of the heart. This has the advantage of providing a broader context than single sections and also a more focused examination than the full 3D heart context. In [Figure 3](#) this partial projection of the ICN localizes a compact population of neuronal clusters with a superior-inferior orientation, distributed on both atria and in the IAS, but preferentially on the left atrium.

By rotating the 3D model, we found that a superior view, i.e., looking down at the base of the heart, provided the ability to distinguish neurons associated with the right versus the left atrium. [Figure 4A](#) takes a superior view of the 3D heart and ICN, viewing the base of the heart from a viewpoint that highlights the profile of the IAS (also see [Video S3](#)). In particular, the distribution of neurons in the left and right atria can be observed in relation to the IAS, with neurons associated with both atria, but more so to the left atrium, with a much smaller population within the IAS itself. In [Figure 4A](#), the entire population of the ICN is seen from a superior viewpoint allowing appreciation of the full distribution of neurons on the left and right atria.

As in rat the ICN is often associated with the hilum on the base of the heart we examined only those neurons with that specific neuroanatomical distribution and localization. In [Figures 4B'](#) and [4B](#) we aim to acquire and then only visualize neurons plausibly located on the base of the heart. As described in previous sections, using "partial projection," a user-defined subset of the 3D heart model and neurons in any plane and thickness can be displayed, more than single sections and less than the full 3D model. Using the partial projection tool, we made a virtual section that displays only neurons at the base of the heart (as seen in [Figure 4B](#)). These ICN neurons are on the epicardial aspect of the base associated with the major pulmonary vessels there at the cardiac hilum. These neurons appear to be on the right atrium and in the IAS.

Our results show that the majority of neurons are positioned more inferiorly to the base of the heart, extending caudally to the boundary with the ventricles as seen in [Figures 2](#) and [3](#). To visualize their distribution and location across the two atria we again took a superior view of the heart to observe left-right neuronal distribution of neurons, but used the Tissue Mapper software "partial projection" tool (to "cut off the base/hilum), and observe only neurons inferior to the base of the heart ([Figure 5](#), [Video S4](#)). This graphic shows those ICN neurons as a transverse or axial visualization of a 3-mm-thick slab of tissue. Neuron clusters are abundant across both atria, but in contrast to the base of the heart neurons are more abundant on the left atrium.

The 3D reference models of the heart and ICN are derived from whole-mount stained histological tissues (i.e., whole rodent hearts). It is also informative to look at these single tissue sections and appreciate the position of

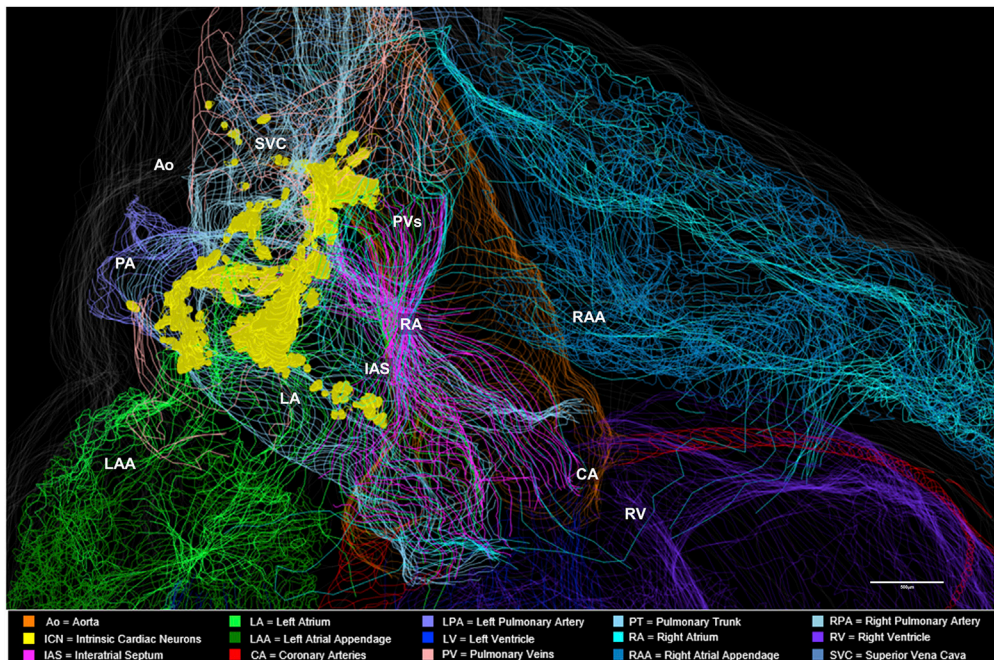


Figure 5. Distribution of More Inferiorly Located ICN

Use of the TissueMapper Partial Projection tool that visualizes the ICN in a 3-mm-thick transverse image slab rotated in a superior view. This illustrates the locations in the transverse plane of section to highlight more inferiorly (caudally) located neurons. Neurons are represented as yellow dots. Scale bar: 500 μm .

the neurons in them. The “native” section images in [Figure 6](#) are from the data acquisition pipeline in [Figure 1A](#). These six tissue section images are at 0.5 μm (x-y) resolution and allow appreciation of the cellular histology for discriminating neurons. As shown at six different levels of the heart ([Figure 6](#)) individual neurons could be identified and their locations determined in relation to the heart chambers and other structures. This heart was sectioned in a near-sagittal plane, and [Figures 6A–6F](#) move sequentially from the right to the left side of the heart. The image volume is available online through the SPARC Data Portal. [Figure 6A](#) is close to the right side limit to the ICN, and [Figure 6F](#) is close to the left limit. The numbers in each panel indicate the right-left position of the section. Thus, [Figure 6A](#) is 1,285 μm from the right heart edge and [Figure 6F](#) is 4,020 μm farther left. In these tissue sections, neurons form clusters on the surface of the walls of the right and left atria. As seen in [Figures 2](#) and [4](#) these clusters continue across many sections, so that when the maps are combined (stacked) across sections, these neurons form somewhat continuous structures in the 3D model. These structures may represent previously identified cardiac ganglionated plexuses ([Cheng et al., 1999, 2004](#)).

The qualitative inspection of ICN clustering finds areas of high and low neuronal packing density, whereas a more quantitative and objective approach to these observations involves use of “partitioning around medoids (PAM)” algorithm to assay packing density or clustering ([Kaufman and Rousseeuw, 1987](#)). These clusters can be viewed in Tissue Mapper in 3D cardiac context ([Figure 7A](#); [Video S5](#)) and without cardiac features, as the ICN alone, in a posterior point of view ([Figure 7B](#)) and in [Figures 7C–7E](#) in rotated points of view to highlight the shapes of the clusters. These clusters can be represented as surface plots, as in [Figure 7F](#), where the height of the surface contour represents the neuronal packing density.

It is possible that, like the neurons in the brain, these clusters of neurons may be somewhat variable in precise spatial distribution from animal to animal, but identifiable as they are consistently present at the coarse-grain anatomical locations relative to notable cardiac features. By analyzing the connectivity and molecular phenotype of individual neurons from these clusters, it may be possible to identify functional groupings within the ICN. They may have a consistent connectome of functionally specific projections and may also have distinct molecular phenotypes. The representation of the anatomy of molecular phenotypes of the ICN requires the data acquisition pipeline described in [Figure 1B](#). [Figures 8](#) and [9](#) show rat heart sections acquired in this pipeline. [Figure 8](#) presents overviews of regions containing ICN neurons

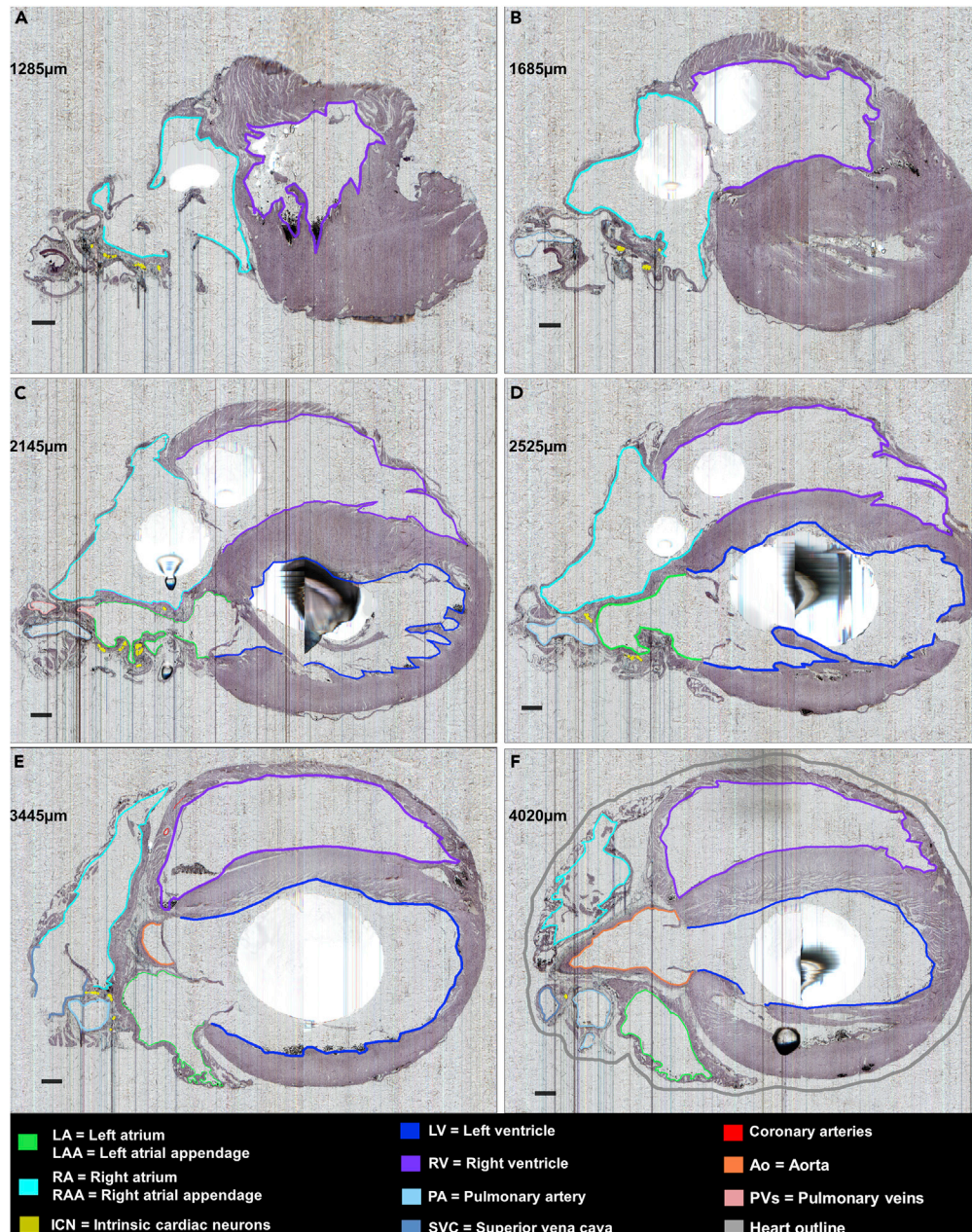


Figure 6. ICN Distribution at Six Different Semi-sagittal Levels of the Heart

(A–F) Histological sampling of the sagittal sections extending from the right to the left side of the heart at the levels indicated in microns in each panel. The neurons are mapped with yellow dots. The contours help to contextualize the distribution of ICN relative to other features of the heart. Sections are 5 μm , images are at 0.5 μm x-y resolution. The black blobs are artifacts of uneven paraffin embedding. Scale bar: 500 μm .

from which laser capture microdissection (LCM) samples were acquired, and [Figure 9](#) the detailed neuronal groupings from which single neurons were sampled.

Combining 3D Anatomical Mapping of the ICN with Laser Capture Microdissection of Single Neurons for Molecular Phenotype Analysis

The sections in [Figures 8](#) and [9](#) are single sections from a female rat heart in which we mapped the 3D organization of the ICN. The heart was sectioned in the transverse plane going rostro-caudally between the

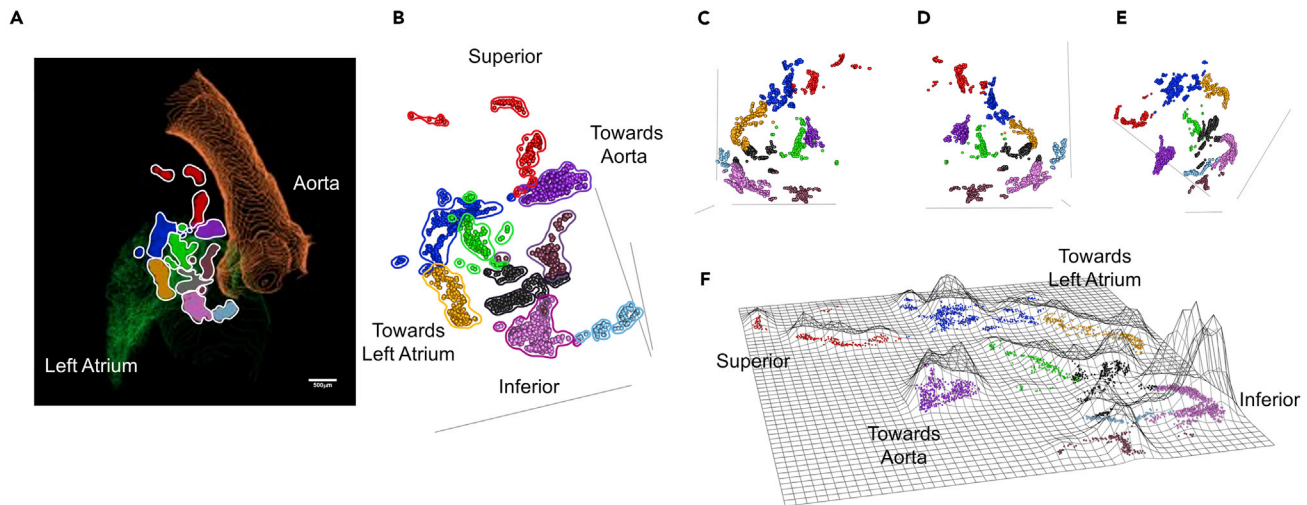


Figure 7. Identification of Neuronal Clusters in the Rat heart

Nine clusters of neurons were identified using the partitioning around medoids (PAM) algorithm, where identified clusters are shown in different colors. (A) Visualization of mapped neurons in their 3D orientation in TissueMapper; contours show the aorta (orange) as well as the left atrium (green). (B) Visualization of mapped neurons in their 3D orientation. (C–E) Visualization of mapped neurons in their 3D orientation rotated to show different points of view. (F) Flat-mount projection of mapped neurons where the height of the contours are proportional to the density of neurons. The orientation in (E) matches the flat-mount projection in (F). (See also [Video S5](#)). Scale bar: 500 μ m.

base and apex. The tissue sections shown are at regular intervals at levels where ICN neurons are present in the heart. At each level the position of captured neurons is indicated in yellow. These distributions in two dimensions are like what is seen in [Figures 2, 3, 4, and 5](#) in 3D or stacks, with relatively continuous distributions of neurons that tend to clump in groups consistent with being described as ganglionated plexuses. Distinct clusters of widely separated cell groups are associated with both atria. Sections are numbered from the base, and neurons were found in sections 39 through 470.

The neurons marked with yellow dots in [Figure 9](#) indicate the single cells mapped within the ICN. An effort was made to select cells randomly but broadly representative across all sections. Neurons that were lifted from the tissue by performing LCM at Z1 levels are marked green ([Figures 9B and 9C](#)), and those from Z2 levels are marked in blue ([Figure 9D](#)). Such microdissected neurons ($n = 151$) were used to perform single-cell transcriptomics. The molecular phenotype of each neuron is associated with the position of each cell in the heart's 3D coordinate framework. The genes expressed and the cell types of these isolated neurons combined back into the specific distributions in 3D context generated by stacking the serial images. This quantitative display can then be used for the visualization of laser capture neurons and linked to their molecular phenotype datasets. [Figures 10A and 10B](#) use the "data-driven" ICN quantitative clustering as was done in [Figure 7](#). However, this ICN was "undersampled" for mapping and is not for comparison to [Figure 7](#). Rather it is to provide context for the clustering and distribution of the ICN neurons lifted for molecular profiling in [Figures 10C and 10D](#) ([Video S6](#)).

Molecular Analysis of Single Neurons in the 3D ICN Context

We obtained a high-throughput transcriptomic dataset containing 23,254 data points from 151 samples of single neurons ([Figure 11](#)). Each sample was assayed for the expression of 154 genes selected as associated with neuromodulation and cardiac function. We analyzed this transcriptomics data using principal-component analysis (PCA) to identify the structured variation that, if present, could organize the neurons into subgroups based on the variability in the gene expression profiles ([Figure 12](#)). We mapped the three major neuron groups that arose from PCA results to their spatial location in the three-dimensional coordinates of ICN. Interestingly, the superior-inferior position (base to apex direction) accounted for the most robust clustering along the first two principal components PC1 and PC2 that account for the top two dominant sources of variation in the gene expression data ([Figure 12A](#)). Samples were divided into three Z position groups (Z1, Z2, Z3) where Z1 is closest to the base, moving down to Z3 near the inferior aspect of the atria

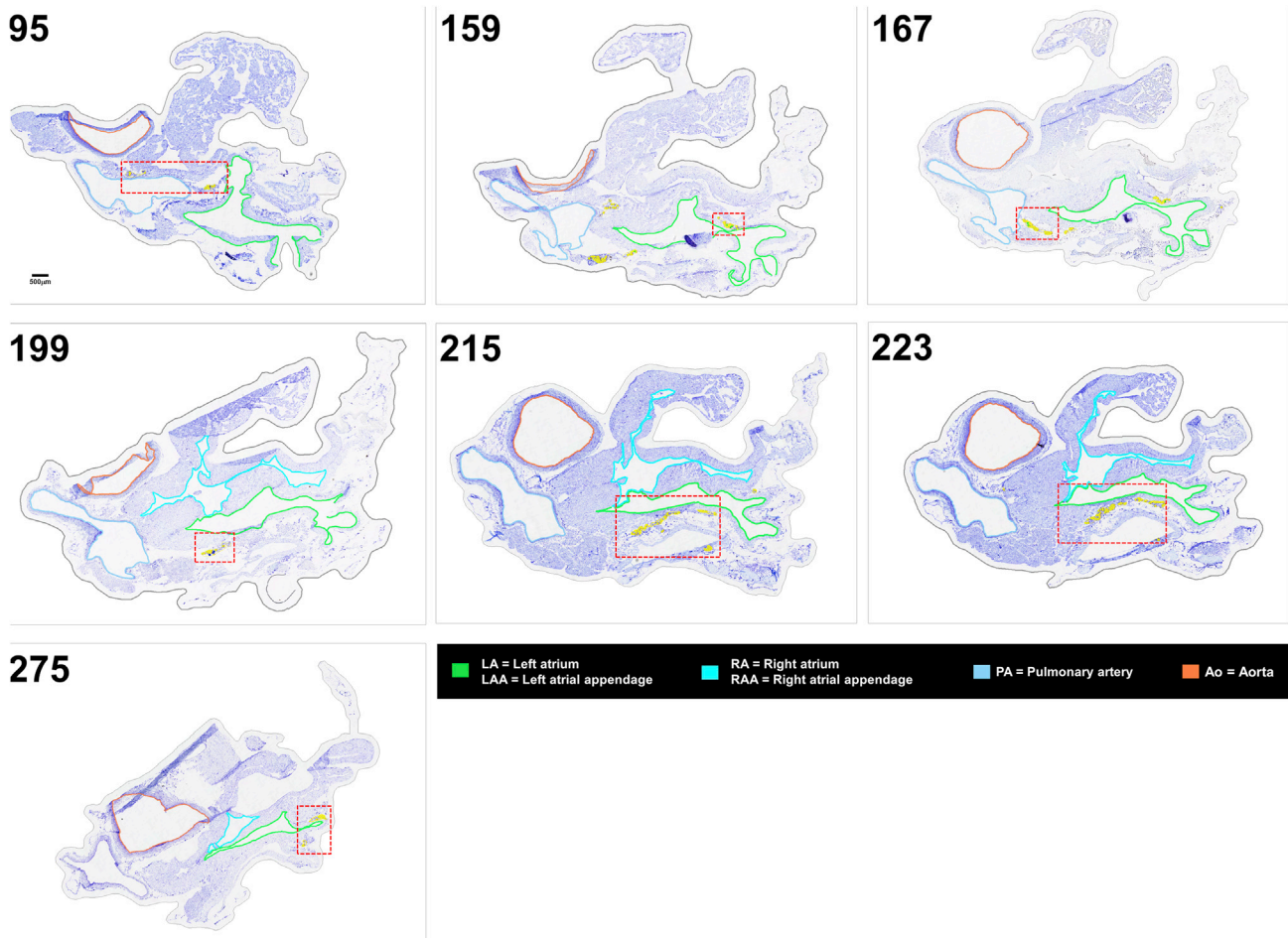


Figure 8. Candidate Sections of Female Rat Heart B to Contextualize the Laser Capture Microdissected Intrinsic Cardiac Neurons

Each of the candidate sections provide additional context for the seven levels of laser capture microdissected neurons. The red boxed areas are the regions of interest that are zoomed in the following figure. Scale bar: 500 μm .

(Figure 12). Examining the gene expression profiles of samples within the Z groups, distinct sets of genes were distinctly enriched in each of the Z1, Z2, and Z3 positional groups, with a small subset being enriched in both Z2 and Z3 (Figure 12C). Notably, the neurons within each of the Z groups were isolated from multiple ganglia (Figure 11), suggesting that the heterogeneity of molecular phenotypes is more constrained than the spatial distribution of these neurons.

We also analyzed the distribution of select molecular profiles in a pairwise fashion to assess the alignment of conventionally described cell types in the ICN. For example, a pairwise comparison of Th and Npy expression demonstrated that whereas several neurons could be classified as Th only or Npy only, a subset of neurons were both Th and Npy positive. These Th⁺ Npy⁺ neurons were distributed throughout ICN without any apparent bias toward a narrow spatial location (Figure 12D, left). These results are consistent with results from immunohistochemistry where NPY-positive cells and TH-positive cells were observed as broadly distributed in the ICN (Richardson et al., 2003), but did not have a correlated expression as was suggested in other results (Crick et al., 1994). Examination of Galanin along with Th, however, shows a more organized pattern with higher expression of Galanin in the Z1 position groups, but with little correlation with Th generally (Figure 12D, right). Interestingly, we found that certain genes showed a very strong spatial localization bias, and examining them in a pairwise manner reveals further co-localization patterns. For example, Cxcr4 and Npff were highly correlated with spatial location. Cxcr4 expression was almost exclusively high in the Z2 and Z3 positional groups, whereas Npff expression was the highest in Z3, was the lowest in Z2, and was mid-range in Z1 (Figure 12D, left). Cxcr4 and Npff were co-expressed in the

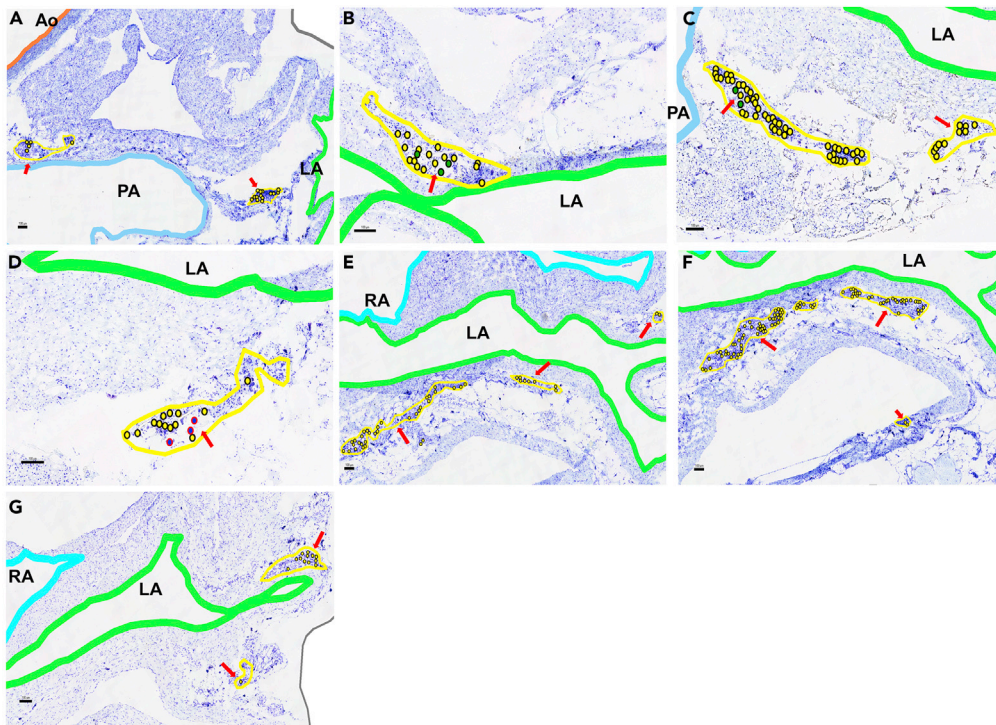


Figure 9. Enlarged Sections of LCM Lifted Intrinsic Cardiac Neurons from Six Different Levels in the Female Rat Heart B

(A) Section 95: Small ganglia located between the aorta, pulmonary artery, and left atrium; all neurons marked yellow.
(B) Section 159: neurons are lifted from a medium ganglia near the left atrium and are grouped in the Z1 molecular cluster; cells marked green.
(C) Section 167: Z1 neurons that are located around the left atrium and pulmonary artery; cells marked green.
(D) Section 199: LCM-sampled neurons that were characterized as the Z2 group were part of a small ganglia; cells marked blue.
(E) Section 215: Neurons were sampled from ganglia near the left atrium and right atrium.
(F) Section 223: LCM-sampled neurons from a large cluster near the left atrium.
(G) Section 275: LCM-sampled neurons around the left atrium. Scale bars: 100 μ m. Red arrows mark the locations of relevant neurons.

neurons in the Z3 positional group. By contrast, the neurons in the Z3 positional group with high expression levels of *Npff* showed distinctively low expression levels of *Dbh*, with little correlation between the two genes in Z1 and Z2 neurons (Figure 12D, right). *Cxcr4* is also known as the NPY3 receptor, suggesting that these neurons may be responsive to NPY+ sympathetic fibers projecting to the heart from the stellate ganglion. *Npff* has been shown to increase heart rate when acting on receptors in the rat heart, working synergistically with adrenergic signaling pathways (Allard et al., 1995). Using the mapping techniques discussed in the previous sections, we can also visualize the expression patterns of these genes within the context of their three-dimensional localization, making it possible for us to delve deeper into the relationship between their expression patterns and locations within the rat ICN (Figure 12F).

We evaluated the gene expression data for differences between the three Z positional groups using a one-way ANOVA with 85 degrees of freedom. Hierarchical clustering of samples using the genes with ANOVA $p < 0.001$ elucidated four subtypes of neurons (Figure 13A–D), with subtypes A and C being found primarily in the Z1 group, B in the Z2 group, and D in the Z3 group along with a number of samples from the Z1 group (Figures 13A and 13B). We analyzed the molecular patterns that underlie the spatially organized neuronal subtypes to identify correlated modules of gene expression and the combinations of modules that distinguish each neuronal subtype. For example, we see that comparing *Npff* to *Cxcr4* expression largely delineates the different phenotypes. We saw that *Npff* and *Cxcr4* greatly correlate with spatial position of the Z groupings, where the Z1 group shows a range of expression of *Npff*. When examining phenotypes, however, we see that phenotype A is largely composed of cells that have low expression of both *Npff* and *Cxcr4*,

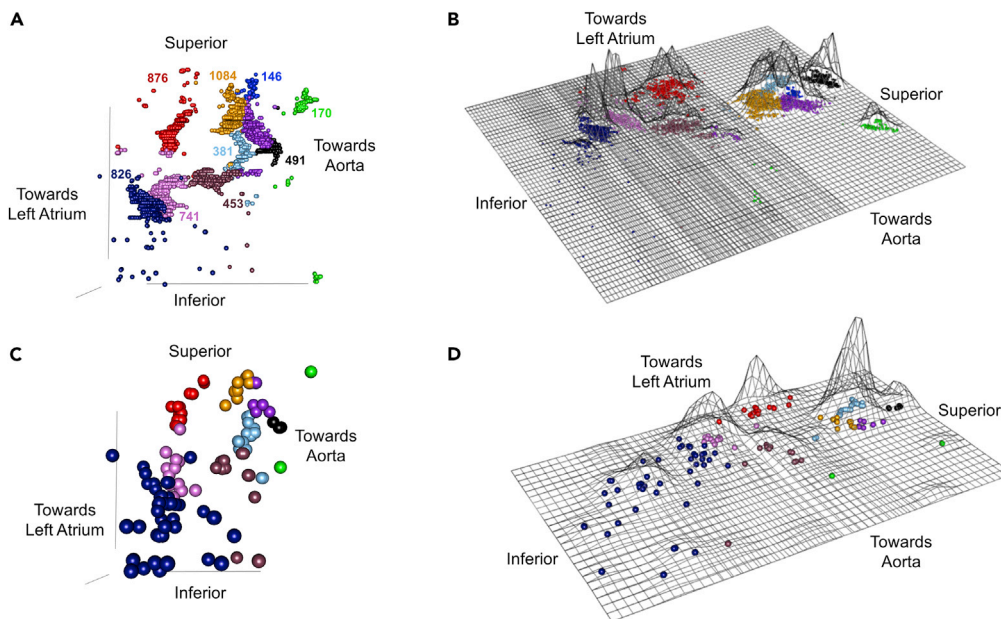


Figure 10. Identification of Neuronal Clusters in the Rat Heart B

(A–D) Visualization of mapped neurons (A) and sampled neurons (C) in their 3D orientation. Flat-mount projection of mapped neurons (B) and sampled neurons (D) where the heights of the contours are proportional to the density of neurons. Ten clusters of neurons were identified using the partitioning around medoids (PAM) algorithm, where identified clusters are shown in different colors. (See also [Video S6](#)).

whereas phenotype C largely accounts for the cells that show high expression in *Npff* and low expression of *Cxcr4*. We also examined the distributions of neuropeptide and corresponding receptor gene expression across the four identified phenotypes. For example, expression patterns between galanin and its receptor, *Galr1*, show that most cells in the phenotype A express high levels of galanin, with a large subset also expressing high levels of *Galr1*, indicating that cells in phenotype A largely drive galanin signaling both through autocrine signaling and acting as the source for paracrine signaling, whereas cells from phenotypes A, B, and C act as the target for paracrine signaling. Most cells in phenotype D showed low expression for both *Gal* and *Galr1* (Figures 13D and 13E). Examining expression patterns between thyrotropin-releasing hormone (*Trh*) and its receptor *Trhr* shows very different cell-cell signaling connectivity patterns when compared with those for galanin. Although a small set of cells from all four phenotypic groups show coexpression of both *Trh* and *Trhr*, the most noticeable pattern is that phenotype B has consistently high levels of *Trh*, but not *Trhr*, indicating that cells in phenotype B primarily act as the source for paracrine signaling between phenotype B and the other three identified phenotypes.

DISCUSSION

Recapitulation of the Major Findings and Their Significance

In this article, we present a method to identify individual neurons in the cardiac ICN and comprehensively record the neurons' relative spatial positions in the heart at micron-scale resolution. Combined with the ability to extract these neurons for downstream applications, we can now understand the gene expression of individual neurons in the ICN in their spatial context. Together, we present an integrated pipeline for cardiac molecular phenotype data acquisition. Here, we also demonstrate the use of KESM (McCormick, 2002), on cardiac tissue for the purposes of making a cardiac atlas at a micron-level resolution. This process and approach can be expanded to other organ systems for the microscopic mapping of neuronal structures.

All these results were made possible by a team science approach involving four groups each providing distinct but necessary technology, as required by the SPARC Program. The approach demonstrated here should be applicable to other organs with intrinsic nervous systems. This approach can also be extended to human hearts in health and in heart failure, seeking neuromodulators involved in regulating heart function. Understanding the cellular and molecular processes governing innervation and the

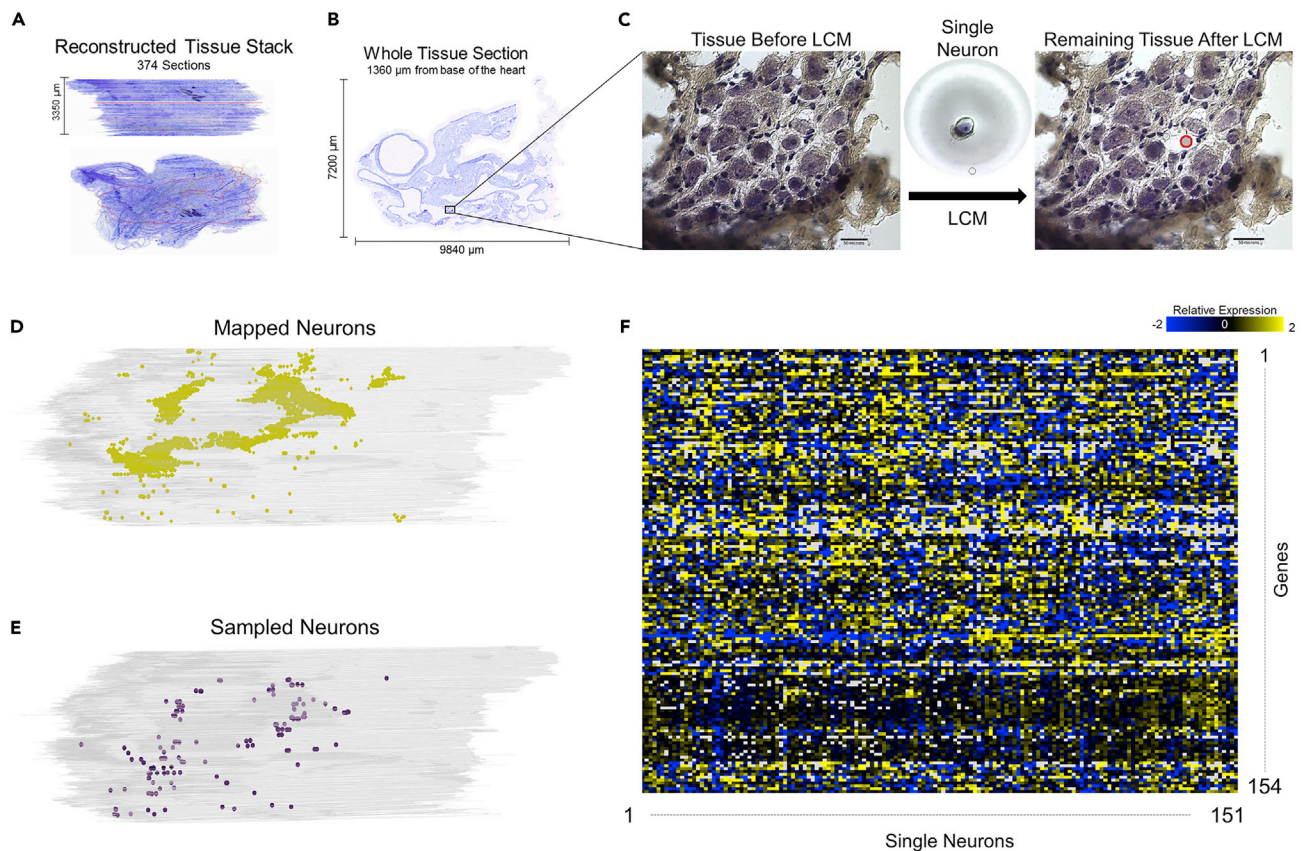


Figure 11. Process of Collecting and Mapping Neurons from the Rat Heart

(A and B) (A) A rat heart was sectioned at 20 μm , imaged, and put into a 3D stack in TissueMaker. The red outline shows a specific section shown in (B). (C–E) (C) The selected region from (B) is shown in a magnified view before and after laser capture microdissection, where the single neuron that has been collected can be seen on the LCM cap (middle). Scale bar: 50 μm . Distribution of mapped neurons (D) and sampled neurons (E) in the context of their 3D location as seen in TissueMapper. (F) Normalized qRT-PCR data showing expression of 154 genes for the 151 samples collected.

functional control of the myocardium in health and disease is the mechanistic basis for the development of neuraxial therapies to prevent sudden cardiac death and arrhythmias (Fukuda et al., 2015). The anatomical and molecular data are all archived in the DAT-CORE Portal of the SPARC Program for public access and use (Tables S1 and S2 and Figure S1). The inspiration for our approach comes from the Allen Institute Brain Atlas, which has been at the forefront of brain sectioning and 3D reconstruction (Lein et al., 2007). Creating a reference framework and mapping anatomical positions of neurons and molecular phenotypes is an ongoing and very active field in brain research, and its extension to the cardiac brain, ICN, benefits from it. Our contribution also resembles reports that provide a data scaffold to enable adding new studies, such as Hsu and Bhandawat (2016).

We find the rat ICN to be a bounded, relatively compact population within the context of the larger 3D anatomy of the heart. It is present on the hilum on the base of the heart, on both the left and right sides, as well as in the IAS. The majority of neurons are on the posterior or dorsal surface of both atria, but more prominently on the left side, extending to the coronary sulcus separating the atria from the ventricles. Within the ICN, neurons tend to cluster and to some extent appear to be continuously distributed in the superior-inferior direction. Quantitative analysis of neuronal packing density suggests several distinct anatomical groupings. The molecular phenotypes of these individual neurons are variable and diverse and reveal many previously unknown neuromodulatory regulators to be present. Spatial analysis suggests that many of these genes have specific gradients of expression, some of which is specifically associated with the neuronal packing density clusters, suggesting functional specificity by molecular phenotype and location within ICN.

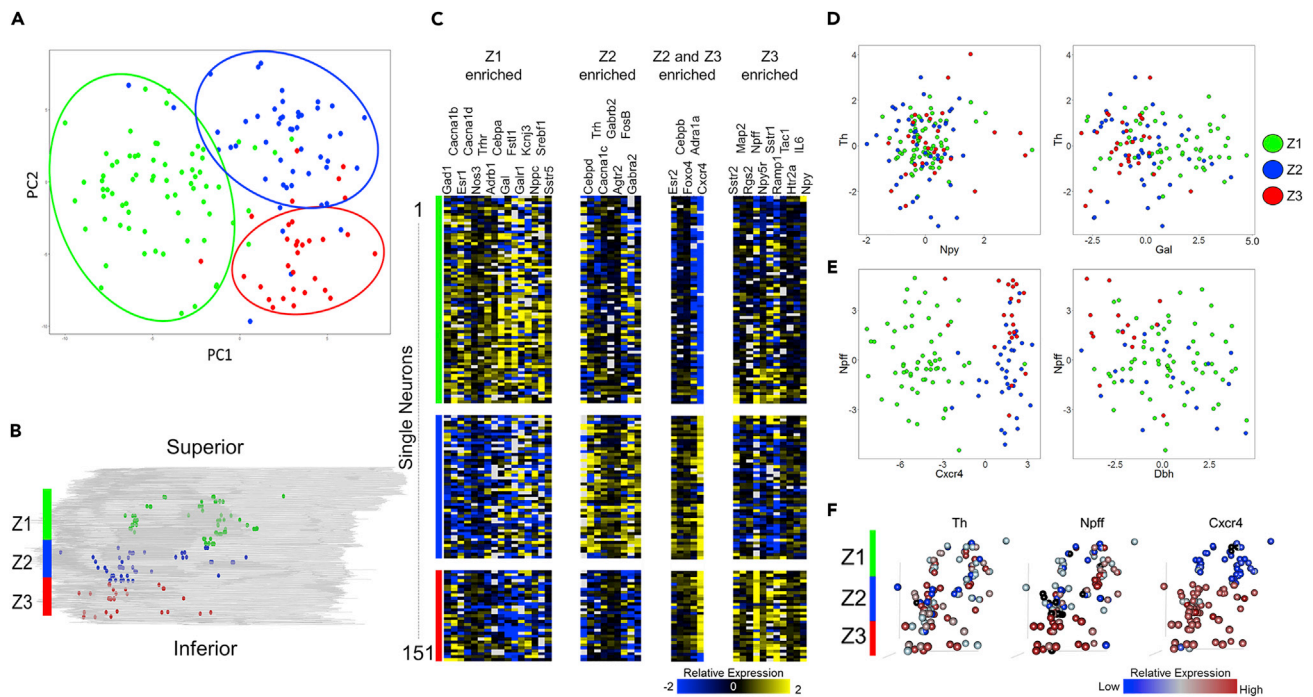


Figure 12. Spatial Gradients of Gene Expression Profiles in the Rat ICN

(A and B) Principal-component analysis (PCA) plot of the 151 collected samples (A) show distinct separation according to their position along the z axis of the heart (B). Samples were divided into three groups along the z axis spanning from Z1 at the base of the heart to Z3 toward the apex. (C) Pavlidis template matching using Pearson correlation with a cutoff of 0.01 was used to find genes that show specific enrichment in one or more Z groups. A cutoff of 0.001 was used to find genes enriched in both the Z2 and Z3 groups to increase specificity. (D) Expression of tyrosine hydroxylase (Th) versus neuropeptide Y (Npy) (left) and Galanin (Gal) (right). (E) Expression of neuropeptide FF (Npff) versus Cxcr4 (left) and Dbh (right). (F) 3D position of collected samples colored for expression of Th, Npff, and Cxcr4. Th (F, left) and Npy (D, left) show little correlation between expression level and spatial location, whereas Galanin (D, right) appears to be upregulated in the Z1 group. Npff (F, middle and E, left) shows downregulation in the Z2 group and distinct upregulation in the Z3 group. Cxcr4 (F, right and E, left) shows very high correlation between expression level and spatial location where expression is significantly downregulated in the Z1 group and significantly upregulated in the Z2 and Z3 groups. Dbh (E, right) shows mixed expression in the Z1 and Z2 groups with low expression in the Z3 group. It can also be seen that Npff and Dbh are anticorrelated in the Z3 group. For all panels, Z1 is represented in green, Z2 in blue, and Z3 in red.

Anatomical Mapping of Intrinsic Cardiac Neurons in the 3D Reconstructed Whole Heart

While qualitative and gross anatomical descriptions of the anatomy of the ICN have been presented, we here bring forth, at a cellular level, a comprehensive atlas, and 3D reconstruction of the ICN in the rat. This work represents a quantum leap in a long history of attempts to understand the anatomical substrate upon which the neuronal control of cardiac function is built. There has not yet been an integrative effort to generate a comprehensive digitized neurocardiac anatomical atlas for any species, or any effort to generate a histological foundation for molecular as well as functional mapping at the single-neuron level for the whole heart of any species.

Prior studies have attempted to map the intrinsic cardiac ganglia, the autonomic afferent and efferent nerve innervation of these cardiac ganglia, and cardiac myocardium. Commonly, immunohistochemical or immunofluorescent staining of a neuronal marker (acetylcholinesterase, tyrosine hydroxylase, choline acetyltransferase, PGP9.5, CGRP, SP) and a fluorescent tracer were used to examine sections, whole mounts, or whole hearts with microscopic or macroscopic organ imaging. Mapping efforts of ICN and cardiac nerve innervation in small animals have included mouse (Ai et al., 2007; Hoard et al., 2008; Li et al., 2010, 2014; Rysevaite et al., 2011a, 2011b), rat (Ai et al., 2007; Cheng et al., 1999, 2004; Cheng and Powley, 2000; Pauza et al., 2000; Richardson et al., 2003), guinea pig (Hardwick et al., 2014; Pauza et al., 2000; Steele et al., 1994), and rabbit (Saburkina et al., 2014; Pauziene et al., 2016). Mapping of ICN was also performed in the hearts of larger animals and humans: dogs (Cardinal et al., 2009; Pauza et al., 2000; Singh et al., 2013; Xi et al., 1991), pigs (Arora et al., 2003; Pauza et al., 2014; Nakamura et al., 2016), and humans

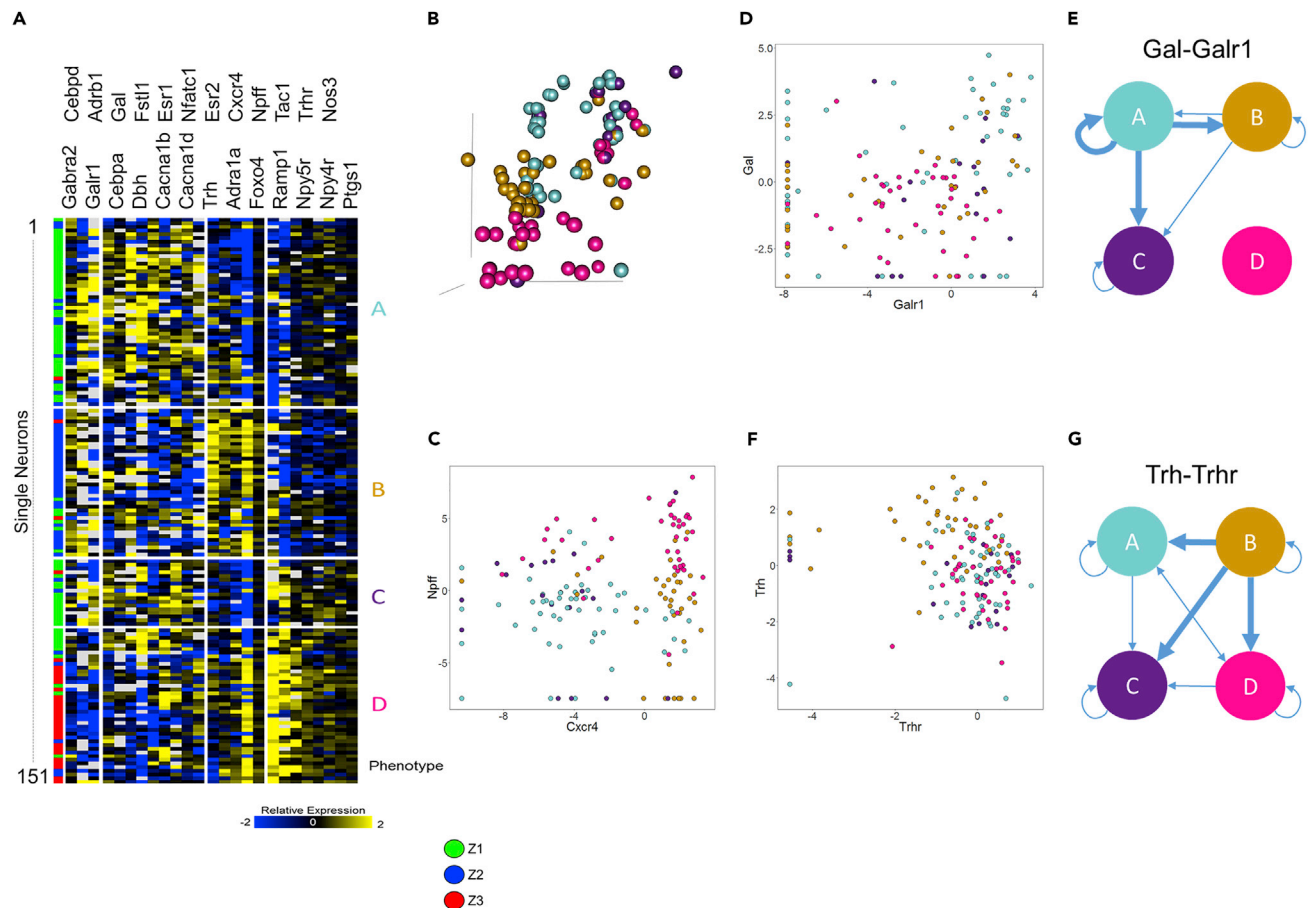


Figure 13. Neuronal Phenotypes Contributing to Spatial Separation

(A) ANOVA was performed with a threshold of 0.001 to find genes that contribute to the separation seen between the three Z groups. Selected genes were clustered using Pearson correlation, resulting in the heatmap shown and giving rise to four different neuronal phenotypes (labeled A–D). We can see that the Z1 group was split into phenotypes A and C, with some samples from the Z1 group clustering along with the Z3 group in phenotype D. Phenotype B is composed mostly of samples residing in the Z2 group.

(B) 3D position of collected samples, colored by phenotype.

(C) Expression of *Npff* versus *Cxcr4*, colored for phenotype. We can see that the comparison of these two genes largely determines the phenotypes.

Phenotype A is mostly composed of cells that have low expression of *Npff* and *Cxcr4*. Phenotype B is composed mostly of cells that have low expression of *Npff* and high expression of *Cxcr4*. Phenotype C is composed largely of cells that have high expression of *Npff* and low expression of *Cxcr4*. Phenotype D is composed largely of cells that have high expression of both *Npff* and *Cxcr4*.

(D) Expression of Galanin versus its receptor *Galr1* and (E) network diagram of putative galanin-mediated connectivity between neuronal phenotypes.

(F and G) (F) Expression of thyrotropin-releasing hormone (*Trh*) and its receptor *Trhr* and (G) network diagram of putative *Trh*-mediated connectivity between neuronal phenotypes.

([Pauza et al., 2000](#); [Petraitiene et al., 2014](#); [Singh et al., 1996, 2013](#)). The ICN in all these species is characterized and summarized by [Wake and Brack \(2016\)](#). With these efforts, either restricted anatomical regions in tissue sections or flat whole mounts were mapped at the microscopic level or large gross anatomical regions were mapped macroscopically.

Although these studies demonstrate the location of the ICN, the extrinsic cardiac innervation by afferent and autonomic nerves, and the intrinsic cardiac innervation, they cannot provide an anatomical substrate for integrating functional and molecular data with anatomically identified ICN neurons in their precise locations in the whole heart. In contrast, our work provides a model to precisely integrate anatomical and molecular data in the 3D digitally reconstructed whole heart with high resolution at the micron scale.

Recent technological advances in tissue clearing techniques make the heart transparent ([Chung et al., 2013](#)). Following tissue clearing, immunohistochemistry and various microscopy techniques can be applied

to map ICN and extrinsic and intrinsic cardiac nerves. Confocal and two-photon imaging requires laser scanning, which is slow and hence practical for only small regions. ICN and extrinsic and intrinsic cardiac nerves may be beautifully imaged with light sheet microscopy, as demonstrated on the murine heart (Ding et al., 2018). This approach can present an ability to create an unbiased view of the myocardium at the single-cell level. However, there appears to be a trade-off between the physical width of the lightsheet (which can determine the axial resolution) and the size of the volume that can be imaged (Richardson and Lichtman, 2015). Hence, lightsheet microscopy with the highest resolution is limited to tissues that are a few hundred micrometers thick. In addition, the electrophoretic process in tissue clearing is not optimal for preservation of charged molecules, including DNA and RNA. Thus, our approach provides a much more comprehensive, reliable, and precise model to integrate anatomical, functional, and molecular data.

Molecular Heterogeneity of Intrinsic Cardiac Neurons: Functional Significance

The current understanding of ICN is that they modulate cardiac physiological functions of chronotropy, dromotropy, inotropy, and lusitropy. Several anatomical studies have hinted at the complexity of cardiac ganglia organization both in the cell body locations (Hasan, 2013; Hoover et al., 2009; Li et al., 2014; Pauziene et al., 2016; Rysevaite et al., 2011a, 2011b; Saburkina et al., 2014) and the complexity of afferent and efferent projections to and from the ICN (Cheng et al., 2004, 1999; Cheng and Powley, 2000; Lin et al., 2014; Li et al., 2014, 2010). Although some work has hinted at the vast heterogeneity of the ICN from a functional perspective (Beaumont et al., 2013), there has not yet been a systematic assay capable of analyzing the molecular substrates that underlies this functional heterogeneity. For example, from a population perspective, it is exactly this type of heterogeneity that may determine the differences between patients who respond to vagal stimulation and those who do not. Furthermore, determination of the deficits in the ICN that drive cardiovascular pathology can lead to new avenues of therapy not only for patients with heart failure but also with an eye toward preventative approaches, as the transition from health to disease is better understood from the perspective of the ICN (Herring, 2015; Longpré et al., 2014). This work elucidates the transcriptional heterogeneity of anatomically positioned ICN in the rat heart, providing anatomical and molecular substrates for functional heterogeneity of cardiac ICNs.

The distinct molecular phenotypes that are defined along the base-to-apex axis have not been previously described. That such an organizational pattern exists may be a result of the embryological development of the intrinsic cardiac ganglia, predominantly from the migration of neural crest cells that differentiate into neurons. The migrating neural crest cells enter the heart at the base and spread out within the atria toward the apex (Fukiishi and Morriss-Kay, 1992; Hildreth et al., 2008). As in the brain, neurons in the heart likely follow chemical gradients to determine the direction and extent of migration, offering a possible explanation for why molecular phenotypes can be defined along the z axis and opening the door for further work to determine which molecules make up these gradients. That cardiac conduction tissues run generally from base to apex may also suggest a functional implication for the separation of neurons in this fashion. In mouse hearts, not all intrinsic cardiac ganglia originate from migrating neural crest cells, especially those that influence nodal pacemakers (Hildreth et al., 2008). Further development of more comprehensive profiling of single neurons within their anatomical context will provide important information as to the role of both neural crest and non-neural crest neurons in the heart.

Data Analysis and Integration Framework

To piece together the relationship between 3D histological reconstructions and single-cell molecular data, data storage and annotation must be carefully considered. The use of an anatomical ontology not only provides a means by which neurons can be anatomically referred to but also makes it so that data from different hearts can be more readily compared. The generation of such data storage and annotation is not a trivial matter and requires collaboration between technicians, researchers, software developers, and data storage specialists. Although purely mathematical and statistical methods for interpreting these data are crucial, the complexity quickly gets to a point where such approaches are challenging, making the ability to qualitatively interpret the data essential. To this end, MBF Bioscience has designed custom software, TissueMaker and Tissue Mapper, allowing for visualization of molecular and anatomical patterns. All processed and raw data are available via the SPARC Data Portal (<https://data.sparc.science>). The data structure adheres to the SPARC data format and is curated by the SPARC data curation team to align the data to community ontologies, to ensure data integrity, and to extract the Minimal Information Standard metadata.

The standardized data will enable mapping onto a 3D scaffold via a common coordinate framework to be used as a reference atlas for comparison across animals as well as across species and experimental conditions. These efforts are presently ongoing in coordination with the MAPCORE group of the SPARC program.

Future Directions for Scalability and Extension

We have established approaches that will now support scaling to acquire several male and female ICN providing a 3D framework as a foundational data resource, useful for developing detailed anatomical neural circuit/connectomic maps for neural control of the heart and showing 3D distribution/gradients of molecular phenotypes. This granularity in the understanding of cardiac neurons has the potential to unlock a new generation of cardiac therapeutics to treat or prevent all forms of cardiac pathology. To achieve the desired integration of different data types, the data from other approaches are visualized within the ICN of the 3D framework. The demonstration of cross-species application of the approach supports scaling to organisms with larger and more complex hearts such as pig and human, and to extension to other organs.

Limitations of the Study

- In the anatomical representations there is some interobserver variability in the manual segmenting. The borders of these anatomic structures depend to some extent on subjective interpretation.
- The single-neuron LCM molecular data collected provide limited, preliminary findings on gradients, heterogeneity, or anatomic patterning. They rest on reliable, replicable multiplexed RT-qPCR, providing substantial but less-than-ideal numbers of samples and depth of gene expression data.
- At this time, single-cell RNA sequencing (RNA-seq) from laser captured cells (regardless of laser capture method) falls short of producing reliable and replicable data. Other single-cell RNA-seq technologies, such as 10x, drop-seq, nuc-seq, and others, necessarily forgo anatomic specificity. As of this writing complex transcriptomic profiling techniques like MERFISH are in their proof-of-concept phases and were not accessible for this work.

Resource Availability

Lead Contact

Further information and requests for resources and reagents should be directed to and will be fulfilled by the Lead Contact, James Schwaber (james.schwaber@jefferson.edu).

Materials Availability

This study did not generate new unique reagents.

Data and Code Availability

Knife-edge scanning microscopy and 3D reconstructed rat heart data: <https://doi.org/10.26275/WOX9-GQZP>.

Laser capture microdissection imaging and molecular profile data: <https://doi.org/10.26275/XMYX-RNM9>.

Knife-edge scanning microscopy (KESM): Strateos, San Francisco, CA: <https://www.strateos.com/kesm/>

Tissue Mapper, Tissue Maker, Biolucida: MBF Bioscience, Williston, VT: <https://www.mbfbioscience.com/tissue-mapper>, <https://www.mbfbioscience.com/tissuemaker>, <https://www.mbfbioscience.com/biolucida>.

Original data have been deposited to SPARC DAT-CORE Data Portal: <https://sparc.science/data?type=dataset&q=heart>.

MAPCORE group of the SPARC program: <https://mapcore-documentation.readthedocs.io/en/latest/RatHeart.html>.

SciCrunch database: <https://scicrunch.org/>.

METHODS

All methods can be found in the accompanying [Transparent Methods supplemental file](#).

SUPPLEMENTAL INFORMATION

Supplemental Information can be found online at <https://doi.org/10.1016/j.isci.2020.101140>.

ACKNOWLEDGMENTS

We would like to thank Dr. Mahyar Osanlouy of the Auckland Bioengineering Institute for ongoing efforts in the process of fitting segmented data to the heart scaffold. Financial support for this work was provided by the National Institutes of Health under the Stimulating Peripheral Activity to Relieve Conditions (SPARC) program, Grant OT2 OD023848 subaward, NHLBI Grant U01HL133360 to J.S.S. and R.V., NIH R15 1R15HL137143-01A1, and NIH 1 U01 NS113867-01 to J.C. The funders had no role in study design, data collection and interpretation, or the decision to submit the work for publication.

AUTHOR CONTRIBUTIONS

Conceptualization, J.S.S., R.V., Z.C., S.T., and J.G.; Methodology, J.S.S., R.V., S.T., N.F., T.H., S.E., Z.C., and J.G.; Software, S.T. and M.H.; Validation, Z.C., C.L., J.C., and L.E.; Formal Analysis, J.G., S.A., A.M., and R.V.; Investigation, J.G., S.A., C.L., S.R., and J.C.; Resources, S.T., M.H., N.F., T.H., and S.E.; Data Curation, J.S.S., A.M., and R.V.; Writing – Original Draft, J.S.S. and J.G.; Writing – Review and Editing, J.S.S., J.G., and R.V.; Visualization, C.L., A.M., S.R., S.T., M.H., and S.E.; Supervision, J.S.S., R.V., and Z.C.; Project Administration, J.S.S.; Funding Acquisition, J.S.S. and R.V.

DECLARATION OF INTERESTS

S.T. and M.H. are paid employees of MBF Bioscience (Williston, VT). S.T. and M.H. are also funded by the NIH Common Fund award, OT3OD025349 to Dr. Shivkumar at University of California Los Angeles (subaward to J.S.S., R.V., J.C.), to create multi-scale, multi-organ, multi-species SPARC map management as a part of SPARC Portal. The software development efforts described in this manuscript preceded integration with SPARC DRC. Owing to intellectual property right restrictions, we cannot provide the Tissue Mapper, Tissue Maker or Biolucida Converter source code or its documentation at this time.

Strateos and MBF Bioscience are commercial entities, and the authors affiliated with them are company employees. The remaining authors declare that no competing interests exist.

Received: January 17, 2020

Revised: March 11, 2020

Accepted: May 1, 2020

Published: June 26, 2020

REFERENCES

- Ai, J., Gozal, D., Li, L., Wead, W.B., Chapleau, M.W., Wurster, R., Yang, B., Li, H., Liu, R., and Cheng, Z. (2007). Degeneration of vagal efferent axons and terminals in cardiac ganglia of aged rats. *J. Comp. Neurol.* 504, 74–88.
- Allard, M., Labrousche, S., Nosjean, A., and Laguzzi, R. (1995). Mechanisms underlying the cardiovascular responses to peripheral administration of NPY in the rat. *J. Pharmacol. Exp. Ther.* 274, 577–583.
- Armour, J.A., Murphy, D.A., Yuan, B.X., Macdonald, S., and Hopkins, D.A. (1997). Gross and microscopic anatomy of the human intrinsic cardiac nervous system. *Anat. Rec.* 247, 289–298.
- Arora, R.C., Cardinal, R., Smith, F.M., Ardell, J.L., Dell'Italia, L.J., and Armour, J.A. (2003). Intrinsic cardiac nervous system in tachycardia induced heart failure. *Am. J. Physiol. Regul. Integr. Comp. Physiol.* 285, R1212–R1223.
- Beaumont, E., Salavati, S., Southerland, E.M., Vinet, A., Jacquemet, V., Armour, J.A., and Ardell, J.L. (2013). Network interactions within the canine intrinsic cardiac nervous system: implications for reflex control of regional cardiac function. *J. Physiol. (Lond)* 591, 4515–4533, <https://doi.org/10.1113/jphysiol.2013.259382>.
- Cardinal, R., Pagé, P., Vermeulen, M., Ardell, J.L., and Armour, J.A. (2009). Spatially divergent cardiac responses to nicotinic stimulation of ganglionated plexus neurons in the canine heart. *Auton. Neurosci.* 145, 55–62.
- Cheng, Y.-F., Chang, Y.-T., Chen, W.-H., Shih, H.-C., Chen, Y.-H., Shyu, B.-C., and Chen, C.-C. (2017). Cardioprotection induced in a mouse model of neuropathic pain via anterior nucleus of paraventricular thalamus. *Nat. Commun.* 8, 826.
- Cheng, Z., and Powley, T.L. (2000). Nucleus ambiguus projections to cardiac ganglia of rat atria: an anterograde tracing study. *J. Comp. Neurol.* 424, 588–606.
- Cheng, Z., Powley, T.L., Schwaber, J.S., and Doyle, F.J. (1999). Projections of the dorsal motor nucleus of the vagus to cardiac ganglia of rat atria: an anterograde tracing study. *J. Comp. Neurol.* 410, 320–341.
- Cheng, Z., Zhang, H., Guo, S.Z., Wurster, R., and Gozal, D. (2004). Differential control over postganglionic neurons in rat cardiac ganglia by NA and DmnX neurons: anatomical evidence. *Am. J. Physiol. Regul. Integr. Comp. Physiol.* 286, R625–R633.

- Chung, K., Wallace, J., Kim, S.Y., Kalyanasundaram, S., Andalman, A.S., Davidson, T.J., Mirzabekov, J.J., Zalocusky, K.A., Mattis, J., Denisin, A.K., et al. (2013). Structural and molecular interrogation of intact biological systems. *Nature* 497, 332–337.
- Crick, S.J., Wharton, J., Sheppard, M.N., Royston, D., Yacoub, M.H., Anderson, R.H., and Polak, J.M. (1994). Innervation of the human cardiac conduction system. A quantitative immunohistochemical and histochemical study. *Circulation* 89, 1697–1708.
- Ding, Y., Bailey, Z., Messerschmidt, V., Nie, J., Bryant, R., Rugonyi, S., Fei, P., Lee, J., and Hsiai, T.K. (2018). Light-sheet fluorescence microscopy for the study of the murine heart. *J. Vis. Exp.* <https://doi.org/10.3791/57769>.
- Fukiishi, Y., and Morriss-Kay, G.M. (1992). Migration of cranial neural crest cells to the pharyngeal arches and heart in rat embryos. *Cell Tissue Res.* 268, 1–8.
- Fukuda, K., Kanazawa, H., Aizawa, Y., Ardell, J.L., and Shivkumar, K. (2015). Cardiac innervation and sudden cardiac death. *Circ. Res.* 116, 2005–2019.
- Hardwick, J.C., Ryan, S.E., Beaumont, E., Ardell, J.L., and Southerland, E.M. (2014). Dynamic remodeling of the Guinea pig intrinsic cardiac plexus induced by chronic myocardial infarction. *Auton. Neurosci.* 181, 4–12.
- Hasan, W. (2013). Autonomic cardiac innervation: development and adult plasticity. *Organogenesis* 9, 176–193.
- Herring, N. (2015). Autonomic control of the heart: going beyond the classical neurotransmitters. *Exp. Physiol.* 100, 354–358.
- Hildreth, V., Webb, S., Bradshaw, L., Brown, N.A., Anderson, R.H., and Henderson, D.J. (2008). Cells migrating from the neural crest contribute to the innervation of the venous pole of the heart. *J. Anat.* 212, 1–11.
- Hoard, J.L., Hoover, D.B., Mabe, A.M., Blakely, R.D., Feng, N., and Paolocci, N. (2008). Cholinergic neurons of mouse intrinsic cardiac ganglia contain noradrenergic enzymes, norepinephrine transporters, and the neurotrophin receptors tropomyosin-related kinase A and p75. *Neuroscience* 156, 129–142.
- Hoover, D.B., Isaacs, E.R., Jacques, F., Hoard, J.L., Pagé, P., and Armour, J.A. (2009). Localization of multiple neurotransmitters in surgically derived specimens of human atrial ganglia. *Neuroscience* 164, 1170–1179.
- Hsu, C.T., and Bhandawat, V. (2016). Organization of descending neurons in *Drosophila melanogaster*. *Sci. Rep.* 6, 20259.
- Kaufman, L., and Rousseeuw, P.J. (1987). Clustering by means of medoids. In *Statistical Data Analysis Based on the L1-Norm and Related Methods*, Y. Dodge, ed. (North Holland Publishing Company), pp. 405–416.
- Lein, E.S., Hawrylycz, M.J., Ao, N., Ayres, M., Bensinger, A., Bernard, A., Boe, A.F., Boguski, M.S., Brockway, K.S., Byrnes, E.J., et al. (2007). Genome-wide atlas of gene expression in the adult mouse brain. *Nature* 445, 168–176.
- Lin, M., Hatcher, J.T., Wurster, R.D., Chen, Q.-H., and Cheng, Z.J. (2014). Characteristics of single large-conductance Ca²⁺-activated K⁺ channels and their regulation of action potentials and excitability in parasympathetic cardiac motoneurons in the nucleus ambiguus. *Am. J. Physiol. Cell Physiol.* 306, C152–C166.
- Li, L., Hatcher, J.T., Hoover, D.B., Gu, H., Wurster, R.D., and Cheng, Z.J. (2014). Distribution and morphology of calcitonin gene-related peptide and substance P immunoreactive axons in the whole-mount atria of mice. *Auton. Neurosci.* 181, 37–48.
- Li, L., Huang, C., Ai, J., Yan, B., Gu, H., Ma, Z., Li, A.Y., Xinyan, S., Harden, S.W., Hatcher, J.T., et al. (2010). Structural remodeling of vagal afferent innervation of aortic arch and nucleus ambiguus (NA) projections to cardiac ganglia in a transgenic mouse model of type 1 diabetes (OVE26). *J. Comp. Neurol.* 518, 2771–2793.
- Longpré, J.-P., Salavatián, S., Beaumont, E., Armour, J.A., Ardell, J.L., and Jacquemet, V. (2014). Measure of synchrony in the activity of intrinsic cardiac neurons. *Physiol. Meas.* 35, 549–566.
- McCormick, D.A. (2002). Cortical and subcortical generators of normal and abnormal rhythmicity. *Int. Rev. Neurobiol.* 49, 99–114.
- Nakamura, K., Ajjjola, O.A., Aliotta, E., Armour, J.A., Ardell, J.L., and Shivkumar, K. (2016). Pathological effects of chronic myocardial infarction on peripheral neurons mediating cardiac neurotransmission. *Auton. Neurosci.* 197, 34–40.
- Pauza, D.H., Rysevaite, K., Inokaitis, H., Jokubauskas, M., Pauza, A.G., Brack, K.E., and Pauziene, N. (2014). Innervation of sinoatrial nodal cardiomyocytes in mouse. A combined approach using immunofluorescent and electron microscopy. *J. Mol. Cell. Cardiol.* 75, 188–197.
- Pauza, D.H., Skripka, V., Pauziene, N., and Stropus, R. (2000). Morphology, distribution, and variability of the epicardial neural ganglionated subplexuses in the human heart. *Anat. Rec.* 259, 353–382.
- Pauziene, N., Alaburda, P., Rysevaite-Kyguoliene, K., Pauza, A.G., Inokaitis, H., Masaityte, A., Rudokaite, G., Saburkina, I., Plisiene, J., and Pauza, D.H. (2016). Innervation of the rabbit cardiac ventricles. *J. Anat.* 228, 26–46.
- Petraitiene, V., Pauza, D.H., and Benetis, R. (2014). Distribution of adrenergic and cholinergic nerve fibres within intrinsic nerves at the level of the human heart hilum. *Eur. J. Cardiothorac. Surg.* 45, 1097–1105.
- Richardson, D.S., and Lichtman, J.W. (2015). Clarifying tissue clearing. *Cell* 162, 246–257.
- Richardson, R.J., Grkovic, I., and Anderson, C.R. (2003). Immunohistochemical analysis of intracardiac ganglia of the rat heart. *Cell Tissue Res.* 314, 337–350.
- Rysevaite, K., Saburkina, I., Pauziene, N., Noujaim, S.F., Jalife, J., and Pauza, D.H. (2011a). Morphologic pattern of the intrinsic ganglionated nerve plexus in mouse heart. *Heart Rhythm.* 8, 448–454.
- Rysevaite, K., Saburkina, I., Pauziene, N., Vaitkevicius, R., Noujaim, S.F., Jalife, J., and Pauza, D.H. (2011b). Immunohistochemical characterization of the intrinsic cardiac neural plexus in whole-mount mouse heart preparations. *Heart Rhythm.* 8, 731–738.
- Saburkina, I., Gukauskienė, L., Rysevaite, K., Brack, K.E., Pauza, A.G., Pauziene, N., and Pauza, D.H. (2014). Morphological pattern of intrinsic nerve plexus distributed on the rabbit heart and interatrial septum. *J. Anat.* 224, 583–593.
- Singh, S., Johnson, P.I., Lee, R.E., Orfei, E., Lonchyna, V.A., Sullivan, H.J., Montoya, A., Tran, H., Wehrmacher, W.H., and Wurster, R.D. (1996). Topography of cardiac ganglia in the adult human heart. *J. Thorac. Cardiovasc. Surg.* 112, 943–953.
- Singh, S., Sayers, S., Walter, J.S., Thomas, D., Dieter, R.S., Nee, L.M., and Wurster, R.D. (2013). Hypertrophy of neurons within cardiac ganglia in human, canine, and rat heart failure: the potential role of nerve growth factor. *J. Am. Heart Assoc.* 2, e000210.
- Steele, P.A., Gibbins, I.L., Morris, J.L., and Mayer, B. (1994). Multiple populations of neuropeptide-containing intrinsic neurons in the Guinea-pig heart. *Neuroscience* 62, 241–250.
- Wake, E., and Brack, K. (2016). Characterization of the intrinsic cardiac nervous system. *Auton. Neurosci.* 199, 3–16.
- Xi, X., Randall, W.C., and Wurster, R.D. (1991). Morphology of intracellularly labeled canine intracardiac ganglion cells. *J. Comp. Neurol.* 314, 396–402.

iScience, Volume 23

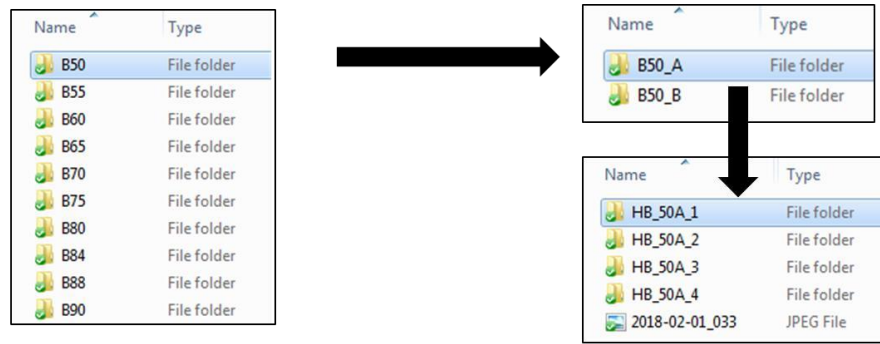
Supplemental Information

A Comprehensive Integrated Anatomical

and Molecular Atlas of Rat

Intrinsic Cardiac Nervous System

Sirisha Achanta, Jonathan Gorky, Clara Leung, Alison Moss, Shaina Robbins, Leonard Eisenman, Jin Chen, Susan Tappan, Maci Heal, Navid Farahani, Todd Huffman, Steve England, Zixi (Jack) Cheng, Rajanikanth Vadigepalli, and James S. Schwaber



Slide #	Slide Region	Sample ID	Cell Count	Overview Image of Section	Image of Area of Interest	Image of Specific Neurons Marked	Image of Cap	Image of Tissue after Neurons Picked	UV laser Marked	UV laser Cut	LCM Date Picked	
1												
2	B50	A	HB_50A-1	10	33	1; 2	3; 4	5; 6	7; 8	34	36	2018-02-01
3	B50	A	HB_50A-2	20	33	9; 10	11; 12	13; 14	15; 16	38	39	2018-02-01
4	B50	A	HB_50A-3	1	33	17; 18	19; 20	21; 22	23; 24	40	41	2018-02-01
5	B50	A	HB_50A-4	5	33	25; 26	27; 28	29; 30	31; 32	35	37	2018-02-01
6	B50	B	HB_50B-1	6	73	32; 43	44; 45	46	47; 48	71	73	2018-02-01
7	B50	B	HB_50B-2	3	73	49; 50	51; 52	53; 56	54; 55	80	81	2018-02-01
8	B50	B	HB_50B-3	6	73	57; 58	59; 60	61; 64	62; 63	75	78	2018-02-01
9	B50	B	HB_50B-4	1	73	65; 66	67; 68	69; 72	70; 71	76	79	2018-02-01

Below the spreadsheet, a row of image thumbnails is shown, each with a date and a number. Arrows from the spreadsheet point to these images:

- 2018-02-01_001 and 2018-02-01_002 (from Overview Image of Section)
- 2018-02-01_003 and 2018-02-01_004 (from Image of Area of Interest)
- 2018-02-01_005 and 2018-02-01_006 (from Image of Specific Neurons Marked)
- 2018-02-01_007 and 2018-02-01_008 (from Image of Cap)
- 2018-02-01_034 and 2018-02-01_036 (from Image of Tissue after Neurons Picked)

Figure S1: Microscopic images are available for all the collected samples, related to Figure 1. In the dataset on the SPARC Data Portal, within the “Samples” folder, there is a document called “Sample_Collection_Information” (Bottom Panel) and another folder titled “Supplementary Sample Acquisition Images”. The top level of this folder is shown on the top panel (left), where the folder names correspond to the slide number of the sample in question (top panel, left and bottom panel, column A). Within that folder is a folder for each slide region (top panel, top right, and bottom panel, column B). Within each folder for a slide region is a folder for each sample containing the images taken for the acquisition of that sample (top panel, bottom right, and bottom panel, column C). For each sample, the corresponding folder contains images showing the area of interest, the neurons marked before they are collected, the neuron after it was collected on the collection cap, the remaining tissue after the neurons had been picked, as well as images showing the tissue before and after an additional UV cut which aided in the mapping of samples later on (bottom panel columns F-K). All images are labeled with the date they were collected followed by a number that is listed in the spreadsheet to identify the images.

TRANSPARENT METHODS

All animal work was approved by the Thomas Jefferson University Institutional Animal Care and Use Committee. Figure 1 illustrates our two approaches as two graphical workflows. We established two multi-component pipelines to map neurons mapped from histological heart tissue sections. One approach (Figure 1A) optimizes precision of 3D heart shape and tissue section alignment for establishing a 3D reference framework. The second (Figure 2B) trades resolution of cardiac structure for, in addition to mapping neuron positions, the acquisition of projections/connectomic data and/or acquisition of neuron samples for molecular profiling.

Figure 1A shows the anatomy-focused pipeline that acquires sections and images by using Knife Edge Scanning Microscopy system (KESM, 3Scan) which maintains precision and eliminates most artifacts greatly improving anatomical rigor and reproducibility. The present results show data from one representative heart from a Fischer (RRID:RGD_1547866; Charles River, USA) 250 g male. Such data supports mapping into a scaffold that provides a reference framework, or atlas, suitable for aligning data from other types of experiments into the 3D structure of the ICN. All 3D model figures in the present work use data from this pipeline, including Figures 2-7.

Figure 1B shows the molecular-focused pipeline, using cryostat sectioning, used here for two 300 g Sprague-Dawley (RRID: RGL_1566457; Envigo, USA) male (Heart A) and female (Heart B) rat hearts. These two hearts were exhaustively cryosectioned producing sections useful not just for comprehensive mapping but also for Laser Capture Microdissection (LCM) of both tracing-labeled and non-connected neurons for transcriptional single neuron profiling. For consistency, the transcriptional profiles of anatomically localized neurons were drawn from one heart, Heart B. Images of these sections, including cell positions, can be stacked to create a whole heart volume with data that can be brought into the 3D reference systems created by the first approach. All transcriptional data and 3D position of these neurons are from Heart B, including Figures 8-13.

Knife Edge Scanning Microscopy

Images taken by KESM have great advantages for precision of gross morphology while resting on cell-level histology, ideal for developing 3D frameworks to hold additional data types from other approaches. Using Tissue Mapper software (MBF Bioscience) to map the position of each neuron as illustrated in Figure 2 we develop a comprehensive mapping of the precise extent and distribution of the ICN in the 3D framework of the heart, as described below:

Sample Preparation: In brief, a normal male rat heart was obtained fresh and subsequently immersed in 4% paraformaldehyde prior to whole-mount diffusion staining with cresyl violet stain (0.05g cresyl echt violet in 50ml dH₂O + 150ul glacial acetic acid, for 7 days) to enable visualization of the intrinsic cardiac neurons and ganglia. The tissue sample was subsequently paraffin embedded and KESM digitized.

Image Acquisition: The FFPE block was KESM digitized at slice thickness of 5 μ m per z-slice. The FFPE block was mounted to a nano-precision XYZ robotic stage. The robotic stage moves samples along the XY axis towards a diamond knife ultramicrotome, which is coupled to a fiber optic cable. Hence, the cutting blade also serves as a source of

illumination. There is custom-built objective, with a 5 mm field of view, and a tube lens that equates to a magnification of approximately 10x trained on the bevel of the diamond knife. The end of the tube lens is coupled to a CMOS TDI line scan color sensor with a 16K pixel resolution RGB output and a 5 μm x 5 μm pixel size.

The 5mm blade moves across the surface of the FFPE block, slicing and scanning simultaneously, capturing one continuous line (or strip) of image data at a time, to generate an image tile comprised of 10,000 pixels, with each pixel representing 0.5 μm . After the strip has been fully sectioned and imaged, the stage is moved to position the adjacent region of the heart in line for sectioning and imaging. This process is repeated until the entire heart has been sectioned.

Image Processing: Post-processing of the data utilizes the precise spatial alignment provided by the KESM technique to generate 2D image planes, which were subjected to denoising and artefact reduction. Individual image planes were assembled together into a 3D volume, enabling quantification of morphological details over large anatomical distances. To achieve this, individual KESM image tiles acquired from each XY location at each Z position were automatically aligned and stitched into 2D image planes, cropped to remove excess image data that did not contain the heart, and then assembled into a 3D image volume with 35:1 JPEG2000 compression using Biolumida Converter. These image volumes were annotated using Tissue Mapper as described below.

Software Development and Neuron Mapping

A custom suite of computational mapping programs have been developed for mapping neurons (or any cell of interest) in organs including the heart: TissueMaker and Tissue Mapper. These were, and continue to be, evolved from the tools MBF Bioscience has developed for brain mapping, such as NeuroLucida and BrainMaker.

The rat heart sectioned at TJU as in Figure 1B was run through the TissueMaker and Tissue Mapper pipeline. By contrast, as in Figure 1A the KESM image data from 3Scan did not require the alignment step in TissueMaker because it was already spatially aligned (see imaging description above).

Using Tissue Mapper software, precise locations of each cardiac neuron were mapped in all sections in which neurons are present. In addition to marking the cell location, numerous regions selected from the comprehensive ontology first generated for the Cardiac Physiome Project (Hunter and Smith, 2016) were mapped. Of the thousands of ontological features that were available, less than 40 were selected for these initial representations in order to simplify the images and to test the pipeline more efficiently. On each section, researchers traced key features (e.g. aorta, pulmonary vessels, atrial borders) and identified neurons based upon a combination of Nissl staining and morphology. The TissueMaker and Tissue Mapper software are then able to generate 3D wireframes of the hearts with neurons positioned in context. Attributes like color and shape can be customized in these reconstructions and quantitative spatial data can be obtained. By mapping anatomical fiducial information alongside the neuron locations,

the extent and location of the neurons within the larger context of the entire heart could be viewed as a 3D representation, as seen in the Figures for the present work.

Cryosectioning and Embedding

In our initial efforts with Heart A (male) and Heart B (female) we learned that, unlike the brain, the distortions of the heart are far less homogenous and symmetric, which can interfere with data visualization and comparison between specimens. Thus we developed the method described below to keep the chambers inflated. We also discovered that the embedding media needs color added to permit image segmentation. Optimal Cutting Temperature media (OCT, TissueTek; VWR 25608-930) is added to an embedding mold, to cover the bottom of the mold and kept on dry ice. Three concentrations of OCT diluted in 1x PBS are prepared 25% 50%, and 100%. The 100% OCT preparation should include a few drops of green food grade dye to permit optimal image segmentation of any subsequent blockface images. The animal is sacrificed using rapid decapitation after 60 seconds of exposure to 5% isoflurane. The heart is immediately excised and submerged in room temperature 1x PBS for 30 seconds or until the majority of blood is pumped out of the chambers. The still beating heart is transferred to 25% OCT, and lightly agitated for 30-60 seconds. This is then transferred to a 50% OCT solution, and lightly agitated for 30-45 seconds. The heart is still beating at this point. The large chambers of the heart were injected with colored OCT via the great vessels using a 14-16 gauge blunt needle on a syringe in order to mitigate structural collapse during cryosectioning. Next, the heart is placed in a chilled embedding mold. Room-temperature OCT is added to completely submerge the heart. The mold is then placed in a slurry of dry ice and methanol to promote rapid freezing. Care was taken to avoid allowing methanol to come into contact with the OCT in the block as this will compromise the structural integrity of the OCT once frozen. Note that holding the block near liquid nitrogen, but not submerging it, is also a means of rapid cooling. After the OCT is completely frozen, it is covered with aluminum foil and then in a plastic wrap to prevent accumulation of condensation in the mold. The mold is transferred to a -80°C freezer. Ideally the entire process should happen within 5-10 minutes to mitigate RNA degradation, which will be necessary for future investigations of single cell transcriptomics using laser capture microdissection.

Slide Preparation and Image Processing

Heart A was sectioned from base to apex at 20µm, yielding nearly 800 sections, with corresponding blockface images, and mounted onto 400 slides (two sections per slide). In order to appreciate a finer level of detail and clarify tissue staining, Heart B was sectioned at 10 µm yielding nearly 1600 sections mounted on 800 slides with blockface images for each section.

Each slide was stained with 0.1% Cresyl violet and dehydrated using increasing concentrations of ethanol and xylene. Cover slips were added using mounting media and slides were then imaged using a slide scanner equipped with 20x Olympus objective (N.A.= 0.75; Bliss-200, MBF Bioscience, Williston, VT). On average, 2,000 image tiles were automatically acquired and stitched to create a high-resolution whole slide image containing two heart sections per image. Using TissueMaker software, the

section images were then extracted from the whole slide image, cropped to a uniform size, the perimeter automatically segmented, and aligned spatially by identifying the centroid of each section to generate an image stack. The heart image volume was then shared with TJU and UCF for further mapping and segmentation using custom-developed software (Tissue Mapper; MBF Bioscience). The software application includes annotation tools for automatically or manually drawing regions, placing markers to indicate cell positions and other discrete points, and the ability to import comprehensive lists of regions as a text or comma-delimited file or via direct integration with the SciCrunch database.

Laser Capture Microdissection of Single Neurons

In order to isolate neurons while maintaining their anatomical origin in three dimensional space, it was necessary to use laser capture microdissection (Arcturus, ThermoFisher). Neurons were visualized using a rapid cresyl violet stain that highlighted the histological appearance of neurons and maintained RNA quality. Single neurons were collected on Capsure HS caps and the cells lysed right on the cap within 15 minutes after laser capture using lysis buffer from the CellsDirect DNA extraction kit (Life Technologies).

Transcriptional assay of laser captured single neurons using multiplex RT-qPCR

RNA-seq performed on laser-captured single cells has only recently been demonstrated and was not available during these experiments (Foley et al. 2019). In order to assay single neurons from laser capture, it was necessary to apply multiplex RT-qPCR to ensure the sensitivity to detect several genes of interest given the small amount of RNA per sample. The Biomark microfluidic system (Fluidigm, San Francisco, CA) was used for all gene expression assays. After reverse transcription and whole transcriptome amplification (Qiagen, Hilden, Germany), the samples were processed through the Biomark system following manufacturer suggested protocols. Quality control of RT-qPCR results included filtering through melt-curve analysis along with automatic C_t thresholding to determine the limit of detection.